RESEARCH ARTICLE

Concentrations, ratios, and sinking fluxes of major bioelements at Ocean Station Papa

Montserrat Roca-Martí[1,2,]*, Claudia R. Benitez-Nelson[3], Blaire P. Umhau[3],
Abigale M. Wyatt[4], Samantha J. Clevenger[1,5], Steven Pike[1], Tristan J. Horner[1],
Margaret L. Estapa[6,7], Laure Resplandy[4], and Ken O. Buesseler[1]

Fluxes of major bioelements associated with sinking particles were quantified in late summer 2018 as part of the EXport Processes in the Ocean from RemoTe Sensing (EXPORTS) field campaign near Ocean Station Papa in the subarctic northeast Pacific. The thorium-234 method was used in conjunction with size-fractionated (1–5, 5–51, and >51 μm) concentrations of particulate nitrogen (PN), total particulate phosphorus (TPP), biogenic silica (bSi), and particulate inorganic carbon (PIC) collected using large volume filtration via in situ pumps. We build upon recent work quantifying POC fluxes during EXPORTS. Similar remineralization length scales were observed for both POC and PN across all particle size classes from depths of 50–500 m. Unlike bSi and PIC, the soft tissue–associated POC, PN, and TPP fluxes strongly attenuated from 50 m to the base of the euphotic zone (approximately 120 m). Cruise-average thorium-234-derived fluxes (mmol m^{-2} d^{-1}) at 120 m were 1.7 ± 0.6 for POC, 0.22 ± 0.07 for PN, 0.019 ± 0.007 for TPP, 0.69 ± 0.26 for bSi, and 0.055 ± 0.022 for PIC. These bioelement fluxes were similar to previous observations at this site, with the exception of PIC, which was 1 to 2 orders of magnitude lower. Transfer efficiencies within the upper twilight zone (flux 220 m/flux 120 m) were highest for PIC (84%) and bSi (79%), followed by POC (61%), PN (58%), and TPP (49%). These differences indicate preferential remineralization of TPP relative to POC or PN and larger losses of soft tissue relative to biominerals in sinking particles below the euphotic zone. Comprehensive characterization of the particulate bioelement fluxes obtained here will support future efforts linking phytoplankton community composition and food-web dynamics to the composition, magnitude, and attenuation of material that sinks to deeper waters.

Keywords: Biological pump, Bioelements, Particulate fluxes, Transfer efficiency, Size-fractionated particles, EXPORTS

1. Introduction

The biological carbon pump redistributes atmospheric carbon dioxide into the ocean interior principally through the formation and export of particulate organic carbon (POC) via a combination of physical and biological processes (Boyd et al., 2019). The biological carbon pump also redistributes many other bioelements, such as particulate nitrogen (PN), total particulate phosphorus (TPP), biogenic silica (bSi), and particulate inorganic carbon (PIC) that play critical roles in a variety of ecological and chemical processes, such as biological production, scavenging of particle-reactive trace elements, and particle export. As these bioelements are cycled through mesopelagic food webs, they may be transformed back into dissolved phases (i.e., remineralized), though not necessarily at the same rate (Arístegui et al., 2009; Twining et al., 2014; Steinberg and Landry, 2017). This remineralization depth controls the distribution of carbon and associated bioelements throughout the water column and determines the time-scale over which these elements are ultimately stored (Kwon et al., 2009). Therefore, accurately quantifying particle flux and attenuation is crucial in order to better understand the factors that control the transfer of material to depth in marine systems.

[1] Department of Marine Chemistry and Geochemistry, Woods Hole Oceanographic Institution, Falmouth, MA, USA

[2] Department of Oceanography, Dalhousie University, Halifax, NS, Canada

[3] School of the Earth, Ocean and Environment, University of South Carolina, Columbia, SC, USA

[4] Department of Geosciences, Princeton University, Princeton, NJ, USA

[5] Department of Earth, Atmospheric and Planetary Sciences, Massachusetts Institute of Technology, Cambridge, MA, USA

[6] Geosciences Department, Skidmore College, Saratoga Springs, New York, NY, USA

[7] Darling Marine Center, School of Marine Sciences, University of Maine, Walpole, ME, USA

* Corresponding authors:
Emails: mrocamarti@whoi.edu; mrocamarti@dal.ca

EXport Processes in the Ocean from RemoTe Sensing (EXPORTS) aims to develop a predictive understanding of the export and fate of global net primary production and associated bioelements and their implications for climate (Siegel et al., 2016; Siegel et al., 2021). This goal requires the use of multiple, complementary approaches to quantify the export of particles from the euphotic zone and subsequent attenuation in the twilight zone across a range of ecosystem states. The first EXPORTS field campaign took place in the northeast Pacific near Ocean Station Papa (Station P; 50°N, 145°W) in August–September 2018. Details on the sampling strategy are found in Siegel et al. (2021). Briefly, two types of ship-based sampling were employed: process-oriented (R/V *Roger Revelle*, RR1813) and survey-oriented (R/V *Sally Ride,* SR1812). The former focused on the characterization of microbial and plankton community structures and ecological and particle flux rates by following a Lagrangian float. The latter sampled for optical and biogeochemical properties as well as particle export over a greater spatial area around the process ship. Sampling on both ships occurred over three time periods spaced 8 days apart, hereafter termed "epochs."

During the EXPORTS campaign in the subarctic NE Pacific, particle fluxes were directly quantified by collecting sinking particles with sediment traps (Estapa et al., 2021) and indirectly using proxies for particle flux, such as thorium-234 (^{234}Th, $t_{1/2} = 24.1$ days). Thorium-234 is a particle-reactive radionuclide that was measured in the upper 500 m of the water column at high spatial and temporal resolution over the three epochs (Buesseler et al., 2020a). The ^{234}Th proxy has been used widely since the 1990s to quantify POC and PN export fluxes over timescales of days to weeks (Buesseler et al., 1992; Le Moigne et al., 2013). To a lesser extent, it has also been used to quantify sinking particle fluxes of biominerals, metals, or contaminants (Gustafsson et al., 1997; Weinstein and Moran, 2005; Le Moigne et al., 2012). This method is based on the quantification of ^{234}Th fluxes from the deficiency of ^{234}Th relative to its conservative parent, uranium-238 (^{238}U, $t_{1/2} = 4.5 \times 10^9$ years), in seawater and the determination of the ratio between POC (or the element of interest) to ^{234}Th associated with sinking particles. The ^{234}Th flux modeling and the ^{234}Th-derived POC fluxes estimated for the first EXPORTS field campaign are described in Buesseler et al. (2020a). Here, we quantified fluxes of other major bioelements (PN, TPP, bSi, and PIC) associated with sinking particles and assessed the biological pump efficiency below the euphotic zone using the ^{234}Th proxy and size-fractionated particles collected by large volume pump filtration during EXPORTS.

2. Methods

2.1. In situ pumps and filter processing
Size-fractionated particles were collected using battery-powered in situ pumps (McLane Industries) coupled to 142-mm diameter "mini-Multiple Unit Large Volume in-situ Filtration System" (MULVFS) style filter holders (Bishop et al., 2012; Lam et al., 2015) deployed from the R/V *Sally Ride* near Station P from August 15 to September 4, 2018 (**Figure 1**; Table S1). Six pumps equipped with two filter
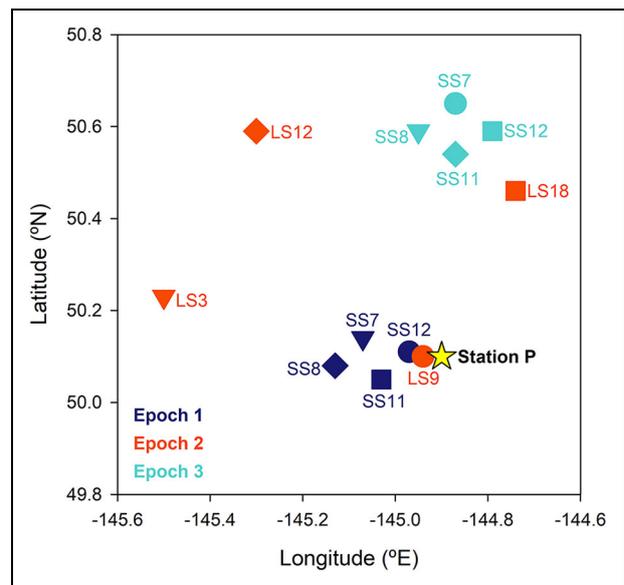
Figure 1. Map of in situ pump stations near Station P. Stations where in situ pumps were deployed near Station P during the EXport Processes in the Ocean from RemoTe Sensing field campaign in August–September 2018. A total of 12 in situ pump casts were conducted over three time periods, spaced 8 days apart, termed "epochs" (Epoch 1 = dark blue, Epoch 2 = red, and Epoch 3 = turquoise). Each symbol represents a specific cast with labels next to the symbols indicating station details: station number and whether it was occupied during a small scale (SS) or large scale (LS) survey (Siegel et al., 2021). DOI: https://doi.org/10.1525/elementa.2020.00166.f1

holders were each deployed for a total of 12 casts (four per epoch) in the euphotic zone (50 and 100 m, $\pm$ 5 m) and the twilight zone (150, 200, 330, and 500 m, $\pm$ 5 m). The base of the euphotic zone (approximately 120 m) was defined by the depth of 0.1% photosynthetic active radiation (PAR; 118 $\pm$ 9 m) and the base of the primary production zone (PPZ; 117 $\pm$ 5 m), defined as the depth where fluorescence declined to 10% of the maximum signal measured in overlying waters (Owens et al., 2015). Pumps were programmed to sample for 4–5 h at a starting flow rate of 8 L min^{-1} and pumped on average 1,600 L.

The filtration system was divided into two flowpaths. On the first flowpath, seawater was passed sequentially through two Nitex screens (51 and 5 μm nominal pore size) followed by a quartz microfiber filter (QMA; 1 μm nominal pore size). Size-fractionated particles from this 3-tier filter system were analyzed for total particulate carbon (PC, includes both POC and PIC), PN, TPP (includes both organic and inorganic phosphorus), bSi (analyzed only on the Nitex screens), PIC, and ^{234}Th. Further subsamples were analyzed for pigments, carbon and nitrogen isotopes, barium isotopic composition, and polonium-210 and lead-210, whose results will be presented elsewhere. On the second flowpath, a 2-tier filter holder was equipped with a 51 μm Nitex screen followed by a polyethersulfone membrane filter (Supor, 0.8 μm nominal pore size) used

for bSi (analyzed only on the Supor filters) and trace metal analyses, as well as bulk and compound-specific isotope analysis of amino acids (which will be presented elsewhere).

Additional filter holders were mounted on the deepest pump to obtain process or "dipped blank" filters from both filter holder configurations (Lam et al., 2015). On the process blanks, a prefilter (0.2 or 0.8 μm Supor) was placed on top of the 51 μm Nitex screen to avoid the collection of particles while filters were exposed to seawater. After recovering the in situ pumps, the prefilter was discarded and the process blanks were processed in the same manner as the samples. During three casts, additional in situ pumps were deployed at 20, 85, and 320 m to allow further analysis of amino acids (presented elsewhere) in four particle size fractions using a single mini-MULVFS filter holder equipped with a 51 and a 6 μm Nitex screen, paired QMA filters, and paired GF75 filters (0.3 μm nominal pore size). A total of five QMA samples from these extra pumps were analyzed for PC, PN, PIC, and [234]Th.

All filter holders were acid-leached prior to the cruise and cleaned after each cast by rinsing with Milli-Q water. Prior to use, QMAs were precombusted at 500 °C for at least 12 h. Nitex screens and Supor filters were acid-leached (10% or 20% HCl; Cutter et al., 2017). Immediately after recovering the pumps, residual water from each filter holder was removed by vacuum. Filter processing was conducted in a clean-air bench (except rinsing of the Nitex screens, see below).

Zooplankton that were not part of the passive sinking flux ("swimmers") and were visible to the naked eye were handpicked from the 51 μm Nitex screens using forceps. At three stations, Nitex screens were cut into "pie-wedges" using a stainless-steel rotary blade (45 mm) to allow for further analyses (Cutter et al., 2017). Particles were gently rinsed off the Nitex screens onto 25-mm diameter 1.2-μm pore-size silver (Ag) filters using 1.0 μm prefiltered seawater. Filtered seawater was kept at 4 °C and was produced once per epoch using 330–500 m seawater. Quartz microfiber filters were subsampled for PC, PN, TPP, PIC, and [234]Th using circular punches of varying size (21–26 mm diameter; Maiti et al., 2012). Samples were dried in a 60 °C oven at sea for several hours, except for two subsets of QMA punches for TPP analysis that were frozen (−20 °C) or stored at room temperature. Supor filters were also frozen (−20 °C or −80 °C) until further processing for bSi.

2.2. Sample analysis
Details regarding [234]Th analyses are provided in Buesseler et al. (2020a). After nondestructive measurement of [234]Th activity on shore, Ag filters were split by weight (Lamborg et al., 2008) into thirds and analyzed for PC and PN, PIC, and bSi.

PC and PN were analyzed using high-temperature combustion at the Woods Hole Oceanographic Institution (WHOI) Nutrient Analytical Facility. Briefly, dried samples of particulate matter were prepared inside an ultraclean tin disk and combusted at high temperature. Carbon was converted into carbon dioxide and nitrogen into nitrogen

gas. These elements were separated by gas chromatography and measured by thermal conductivity on an Elemental Microanalysis Flash EA 1112 (Ehrhardt and Koeve, 1999). PIC was determined by closed-system digestion with phosphoric acid by coulometry (Honjo et al., 1995). POC was obtained from the difference between blank-corrected PC and PIC results.

Analyses of TPP on dried and frozen QMA punches were conducted using a modification of the Aspila phosphomolybdate method (Aspila et al., 1976; Benitez-Nelson et al., 2007b) at the University of South Carolina (UofSC). In brief, filters were combusted at 550 °C to convert any organic phosphorus to inorganic phosphorus and extracted using 1.2 M hydrochloric acid (Aspila et al., 1976). To monitor run-to-run variability and validate analytical accuracy, standard reference materials of tomato leaves (NIST# 1573a) and estuarine sediment (NIST# 1646a) were analyzed with each run (Benitez-Nelson et al., 2007b). Additional TPP analyses were conducted on QMA punches and screen subsections (1/10) that were stored at room temperature at WHOI. Filters were leached with 0.6 M hydrochloric acid at 60 °C for approximately 16 h (Bishop and Wood, 2008). Leachates were reconstituted in 2% nitric acid (by volume), doped to an indium concentration of 1 ng mL^{-1}, and analyzed for multielement concentrations using a Thermo Scientific iCAP quadrupole inductively coupled plasma mass spectrometer (ICP-MS) situated at the WHOI Plasma Facility. Quantification of TPP was achieved via comparison of blank- and drift-corrected sample ion beam intensities to those of reference solutions containing known TPP concentrations. Several samples were measured using both the Aspila and ICP-MS methods (see Section 2.3).

To determine bSi content, filters were extracted in 0.2 M NaOH for 1 h at 95 °C and then neutralized with 1 M HCl (Brzezinski and Nelson, 1989). Subsamples were analyzed for dissolved silicate on the same day using a UV-Visible Spectrophotometer (UV-2550, Shimadzu), following standard spectrophotometric methods (Strickland and Parsons, 1972). bSi was measured on a subsection (1/8) of the Supor filters (2-tier filter holder, 0.8–51 μm) and the Nitex screens (3-tier filter holder, 5–51 μm and >51 μm). Therefore, the analog of the small size fraction for bSi was obtained from the difference between that measured in the 0.8–51 μm and 5–51 μm fractions (for simplicity referred to as 1–5 μm). Hereafter, we refer to each particle size fraction as small (1–5 μm), midsized (5–51 μm), and large (>51 μm).

2.3. Uncertainties and quality control
For all parameters, the average of the process blanks was subtracted from each measurement before dividing by the filtered volume. Process blanks were also used for the determination of uncertainty and limit of detection (Lam et al., 2018). **Table 1** shows the absolute and relative contribution of the blanks for each sample type and parameter. Blanks contributed on average <5% of the total signal of PC, PN, bSi, and [234]Th in all size classes and TPP in midsized and large particles. However, blanks were on average 31% of TPP in the small size class and 42%–

Table 1. Blank correction. DOI: https://doi.org/10.1525/elementa.2020.00166.t1

Parameter	Units	Filter Type	Fraction Analyzed (%)	Size Class (μm)	Avg. $\pm$ SD	% Contribution to Samples, Avg. (Min–Max)	Limit of Detection[a]
Small particles							
Particulate carbon	μmol C	QMA (142 mm)	2.7	1–5	0.15 ± 0.21 ($n = 3$)	1.0 (0.3–3.5)	0.63
Particulate nitrogen	μmol N	QMA (142 mm)	2.7	1–5	0.09 ± 0.05 ($n = 3$)	3.8 (1.2–14)	0.15
Total particulate phosphorus	μmol P	QMA (142 mm)[b]	2.7	1–5	0.053 ± 0.017 ($n = 3$)	31 (13–79)	0.05
Biogenic silica	μmol Si	Supor (142 mm)	12.5	0.8–51	0.06 ± 0.03 ($n = 12$)	3.3 (1.4–19)	0.08
Particulate inorganic carbon	μmol C	QMA (142 mm)	2.7	1–5	0.23 ± 0.01 ($n = 3$)	42 (16–100)	0.04
Thorium-234	dpm	QMA (142 mm)	4.2	1–5	0.13 ± 0.06 ($n = 3$)	1.1 (0.6–1.7)	0.18
Midsized and large particles							
Particulate carbon	μmol C	Ag (25 mm)	33.3	5–51, >51	0.17 ± 0.28 ($n = 6$)	1.5 (0.5–10)	0.83
Particulate nitrogen	μmol N	Ag (25 mm)[c]	33.3	5–51, >51	<0.03 ($n = 6$)	—	—
Total particulate phosphorus	μmol P	Nitex screen (142 mm)[d]	10.0	5–51, >51	5.8 ± 2.6 ($\times 10^{-4}$; $n = 4$)	1.5 (0.4–5.1)	$7.7 \cdot \times 10^{-4}$
Biogenic silica	μmol Si	Ag (25 mm)	33.3	5–51, >51	0.03 ± 0.02 ($n = 6$)	0.8 (0.1–9.1)	0.06
Particulate inorganic carbon	μmol C	Ag (25 mm)	33.3	5–51, >51	0.47 ± 0.03 ($n = 6$)	82 (16–100)	0.10
Thorium-234	dpm	Ag (25 mm)	100	5–51, >51	0.15 ± 0.11 ($n = 6$)	0.8 (0.2–7.4)	0.34

QMA = quartz microfiber filter.

[a]Defined as 3 times the standard deviation of the process blanks.

[b]Dried QMA punches analyzed at the University of South Carolina (see Section 2.2).

[c]Process blanks for particulate nitrogen in midsized and large particles were below the instrumental limit of detection (no blank correction).

[d]Nitex screen subsections analyzed at the Woods Hole Oceanographic Institution (see Section 2.2).

82% of PIC in all size classes. Blank-corrected TPP results were below the limit of detection (3 × standard deviation of the process blanks) in 16% of the samples for the small size class. Blank-corrected PIC results were below that limit in 12%, 94%, and 40% of the samples for small, midsized, and large particles, respectively, given the low PIC concentrations measured. Concentrations below the limit of detection were excluded from data analysis. As such, average PIC concentrations should be considered maximum estimates.

Data for each parameter have an associated uncertainty obtained by propagating the uncertainties from the blank correction (i.e., standard deviation, **Table 1**), and other sources of error including the weighing error of the analytical balance used for splitting the Ag filters (i.e., PC, PN, PIC, bSi in midsized and large particles), and measurement of ^{234}Th.

Triplicate QMA punches from two samples (50 and 500 m) were measured for PC, PN, TPP, and PIC, with a relative standard deviation (RSD) of 1%–5%, 6%–8%, 2%, and 4%–5%, respectively (Table S2). These values indicate that particle distribution was relatively even across the QMA filters and support the reproducibility of the subsampling method (Maiti et al., 2012). In addition, the analytical precision for bSi was determined to be 0.1% based on five consecutive measurements of the same samples in the spectrophotometer.

We further conducted a TPP intercomparison of three subsets of QMA punches from three pump casts that were preserved differently (dried, frozen, room temperature) and analyzed using the two different techniques described above at the UofSC (dried, frozen) and WHOI (room temperature). The results show good agreement between the three subsets of filters (RSD 2%–19%; Figure S1). Here, we use only the results from the QMA punches dried at sea, as data from punches preserved frozen or at room temperature were not available for all stations. However, we use the TPP data from the screen subsamples stored at room temperature and analyzed by ICP-MS, as these samples were only measured using this method.

Seven >51 μm samples were likely contaminated by the presence of swimmers as indicated by high POC/^{234}Th ratios (see Buesseler et al., 2020a). We therefore excluded the POC, PN, and TPP data for these samples. The complete data set can be found at the SeaBASS data repository (https://seabass.gsfc.nasa.gov/archive/WHOI/buesseler/EXPORTS/EXPORTSNP/archive/).
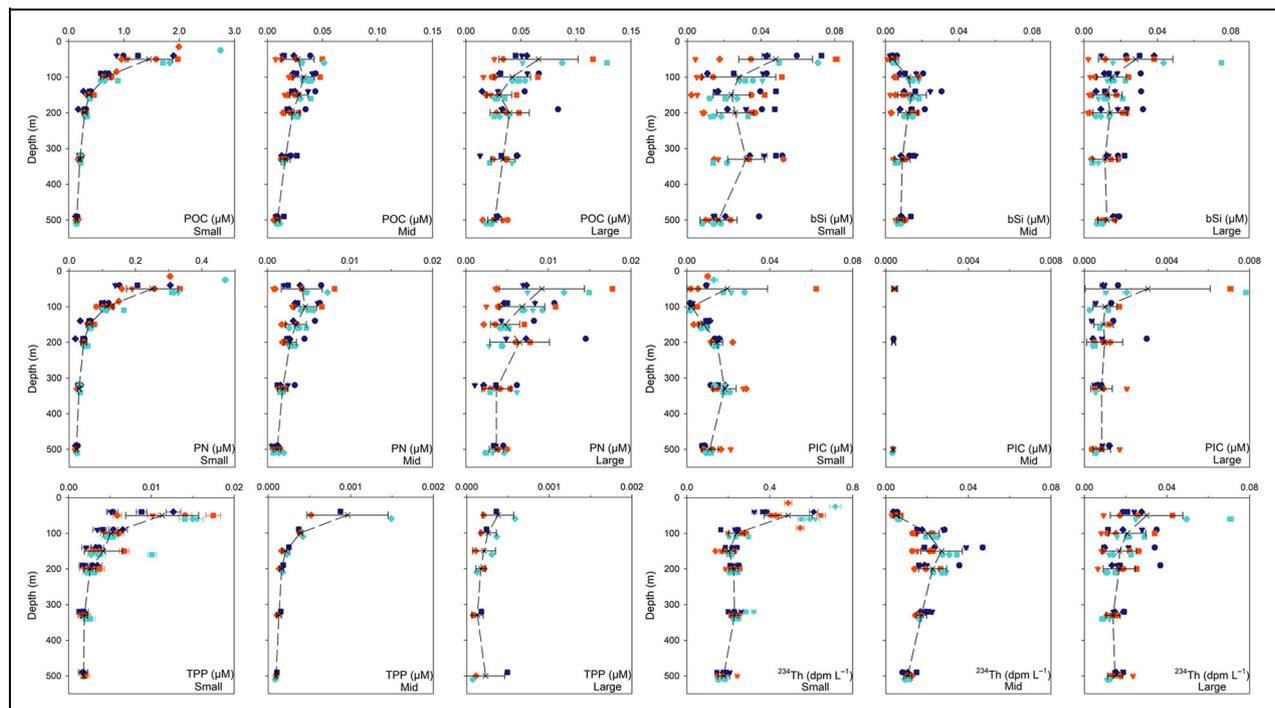
Figure 2. Size-fractionated concentrations of bioelements and thorium-234 (^{234}Th) versus depth. Particulate organic carbon (POC), particulate nitrogen (PN), total particulate phosphorus (TPP), biogenic silica (bSi), particulate inorganic carbon (PIC), and ^{234}Th concentrations versus depth in small (1–5 μm), midsized (5–51 μm), and large (>51 μm) particles collected during the EXport Processes in the Ocean from RemoTe Sensing cruise near Station P. Each symbol represents a specific in situ pump cast color-coded by sampling "epoch" (Epoch 1 = dark blue, Epoch 2 = red, and Epoch 3 = turquoise), as in **Figure 1**. Data from each epoch are offset by 10 m to facilitate visualization. In most cases, error bars are not visible because they are smaller than the symbols. Error bars were obtained by propagating the standard deviation of the process blanks and other sources of error (see Section 2.3). Black crosses show average (±standard deviation) concentrations at 50, 100, 150, 200, 330, and 500 m. Five additional data points for POC, PN, PIC, and ^{234}Th in small particles from 20, 85, and 320 m (Epochs 2 and 3) are shown on the left panels. Note different scales on the x-axes between small versus midsized and large particles, except for bSi. DOI: https://doi.org/10.1525/elementa.2020.00166.f2

3. Results

### 3.1. Profiles of major bioelements and ^{234}Th in size-fractionated particles

POC and PN concentrations in small particles were an order of magnitude higher than those measured in midsized and large particles (**Figures 2** and **3**). In small particles, POC concentrations were on average (±standard deviation) 1.4 ± 0.4 μM ($n = 11$) at 50 m decreasing to 0.144 ± 0.016 μM ($n = 12$) by 500 m, with the largest decline (factor of 4) occurring between 50 and 150 m. Over that 100-m depth range, POC concentrations in large particles also decreased but to a lesser degree (factor of 2), while POC concentrations in midsized particles were relatively constant. The relative contribution of midsized and large particles to POC concentrations increased between 50 and 500 m by a factor of 3 and 4, respectively (**Figure 3**). Variability in POC concentrations was highest at 50 m for the three particle sizes (RSD = 29%–55%), decreasing in deeper waters especially for small particles (RSD < 14%). PN concentrations in the smallest particle size were on average 0.25 ± 0.08 μM ($n = 11$) at 50 m and declined to 0.022 ± 0.003 μM ($n = 12$) by 500 m, showing the same distribution with depth as POC (**Figures 2**–**4**). PN

vertical distribution in midsized and large particles also resembled that of POC.

Concentrations of TPP were also an order of magnitude higher in small particles compared to midsized and large particles, with maximum values at 50 m (0.011 ± 0.004 μM, $n = 11$; 0.0010 ± 0.0005 μM, $n = 3$; 0.0004 ± 0.0002 μM, $n = 3$; respectively; **Figures 2** and **3**). TPP concentrations decreased by a factor of 2 from 50 to 100 m for small and midsized particles but did not change significantly with depth for large particles (one-way analysis of variance [ANOVA], $P = 0.578$). The relative amount of TPP associated with the large size class increased by a factor of 4 from 50 to 500 m as observed for POC and PN (**Figure 3**).

Unlike the soft-tissue elements, bSi concentrations were similar across all particle sizes and varied significantly throughout the water column (RSD = 27%–72%; **Figures 2** and **3**). The highest bSi concentrations were found in small particles, decreasing from an average of 0.05 ± 0.02 μM ($n = 11$) at 50 m to 0.017 ± 0.008 μM ($n = 12$) by 500 m. The largest decline (factor of 2) occurred between 50 and 100 m and between 330 and 500 m. Large particles showed a similar decline from 50 to
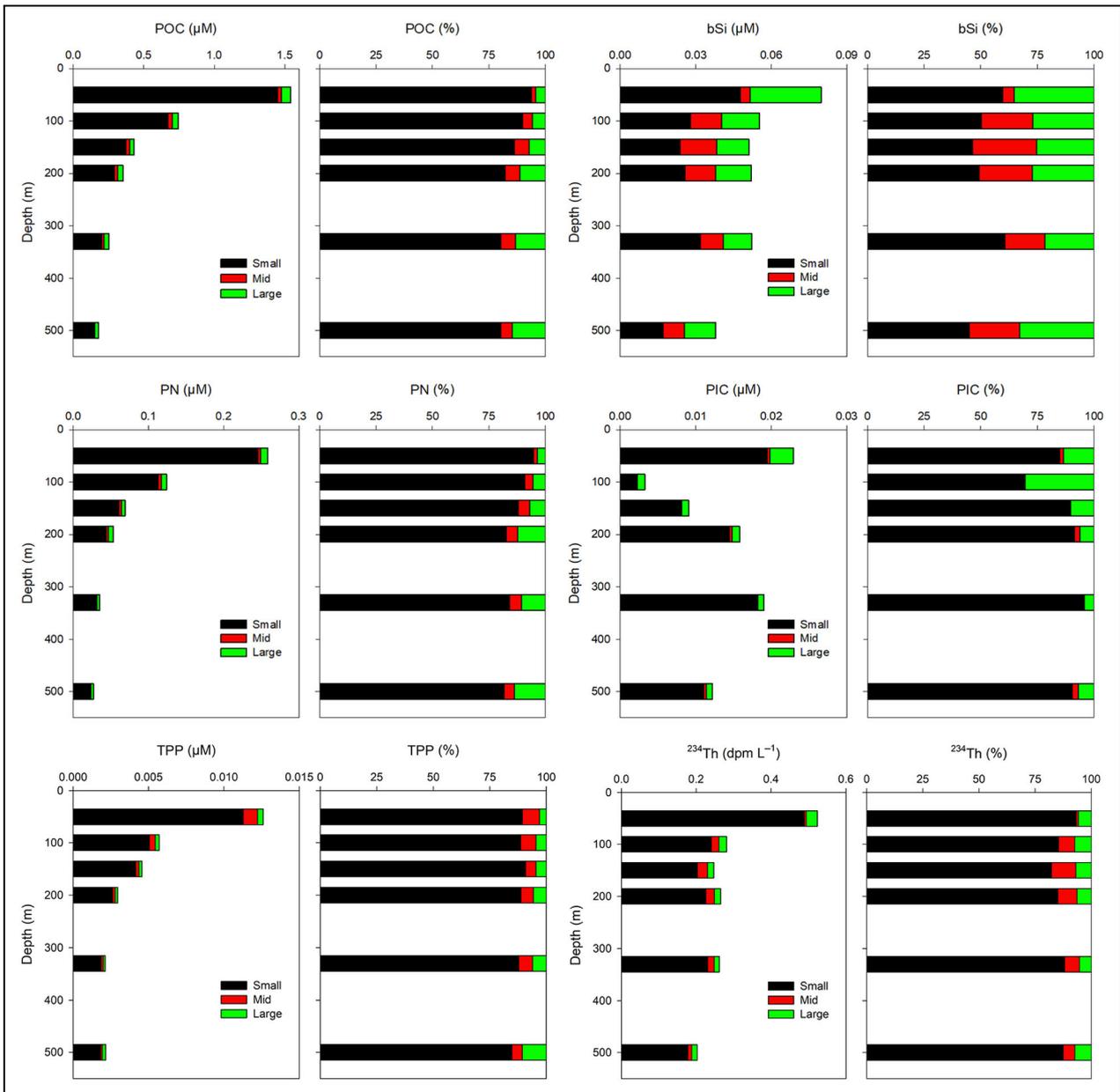
Figure 3. Cruise-average size-fractionated concentrations of bioelements and thorium-234 (^{234}Th) versus depth. Cruise-average particulate organic carbon (POC), particulate nitrogen (PN), total particulate phosphorus (TPP), biogenic silica (bSi), particulate inorganic carbon (PIC), and ^{234}Th concentrations versus depth in small (1–5 μm, black), midsized (5–51 μm, red), and large (>51 μm, green) particles. The left and right panels for each element show the absolute and relative concentrations, respectively, across particle size classes. DOI: https://doi.org/10.1525/elementa.2020.00166.f3

100 m, while bSi concentrations in midsized particles increased over this depth range. Below 100 m, bSi concentrations in midsized and large particles were relatively constant and comparable between both size classes (Mann–Whitney rank-sum test, $P = 0.236$). The combined contribution of midsized and large particles to bSi concentrations was similar to small particles between 100 and 200 m (t test, $P \geq 0.078$) and exceeded that of small particles at 500 m (t test, $P = 0.003$; **Figure 3**).

Concentrations of PIC spanned 3 orders of magnitude, with the distribution among particle size classes being: small > large > midsized (**Figure 3**). Variability was especially high at 50 m (RSD of approximately 100%; **Figure**

2). At 100 m, the relative contribution of small particles to PIC concentrations was smaller than in deeper waters due to a greater contribution from the large size class (**Figure 3**). All but four midsized particulate samples were below the limit of detection. PIC concentrations represented on average <4% of the PC measured in all particle size classes and depths, except between 200 and 500 m, where PIC contributed up to 7% of the PC measured in small particles.

Activities of ^{234}Th were an order of magnitude larger in small particles compared to midsized and large particles, as observed for POC, PN, and TPP (**Figures 2** and **3**). In small and large particles, the highest activities were found
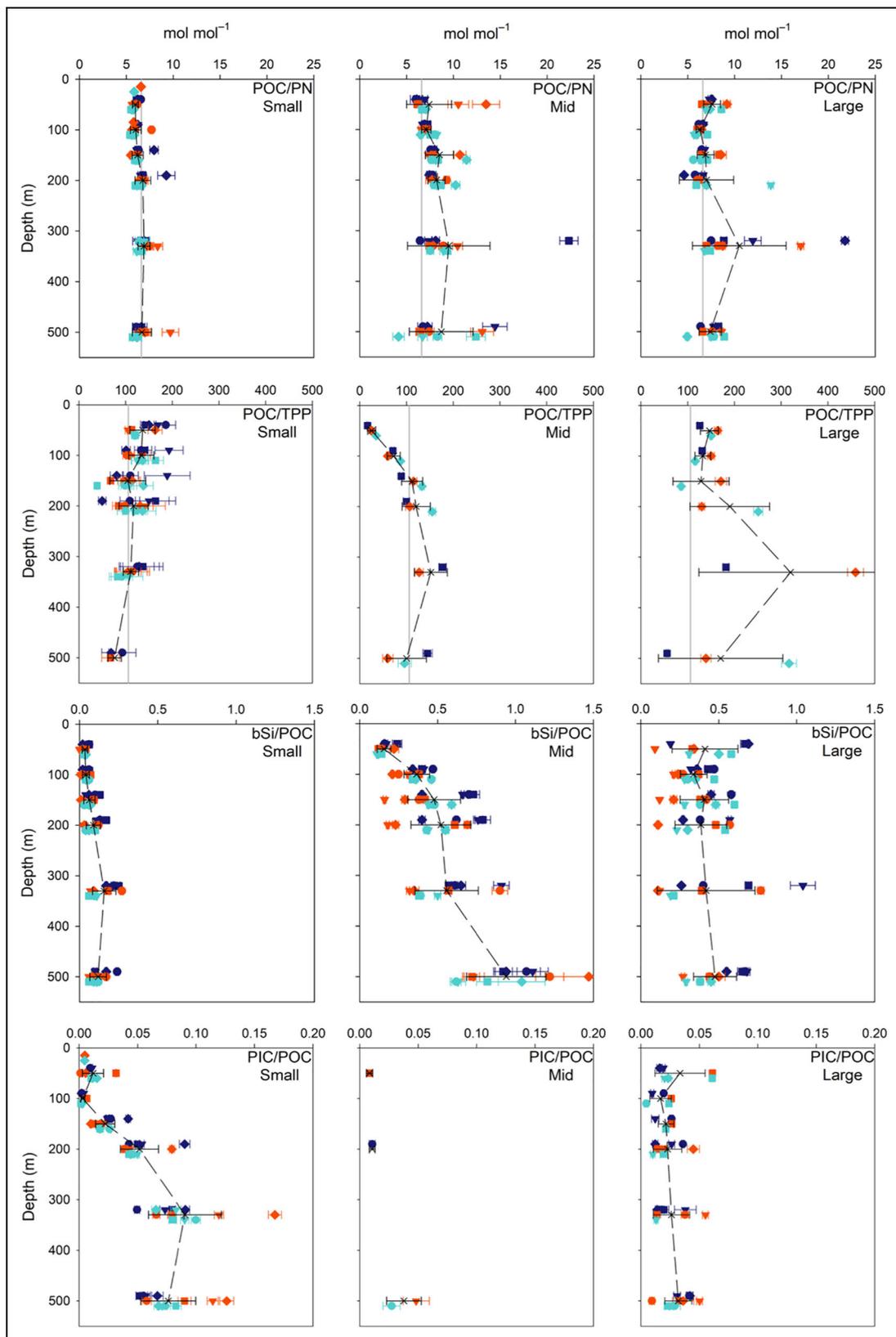
Figure 4. Size-fractionated molar ratios versus depth. Molar ratios of particulate organic carbon (POC)/particulate nitrogen (PN), POC/total particulate phosphorus (TPP), biogenic silica (bSi)/POC, and particulate inorganic carbon (PIC)/POC in small (1–5 μm), midsized (5–51 μm), and large (>51 μm) particles. The same horizontal scales are used for each size class but differ among elements. Each symbol represents a specific in situ pump cast color-coded by sampling "epoch" (Epoch 1 = dark blue, Epoch 2 = red, and Epoch 3 = turquoise), as in **Figure 1**. Error bars were obtained by propagating the uncertainties of POC and the other bioelement considered for each molar ratio. Black crosses show average (±standard deviation) ratios. Vertical gray lines in POC/PN and POC/TPP panels show the Redfield ratio for reference. DOI: https://doi.org/10.1525/elementa.2020.00166.f4
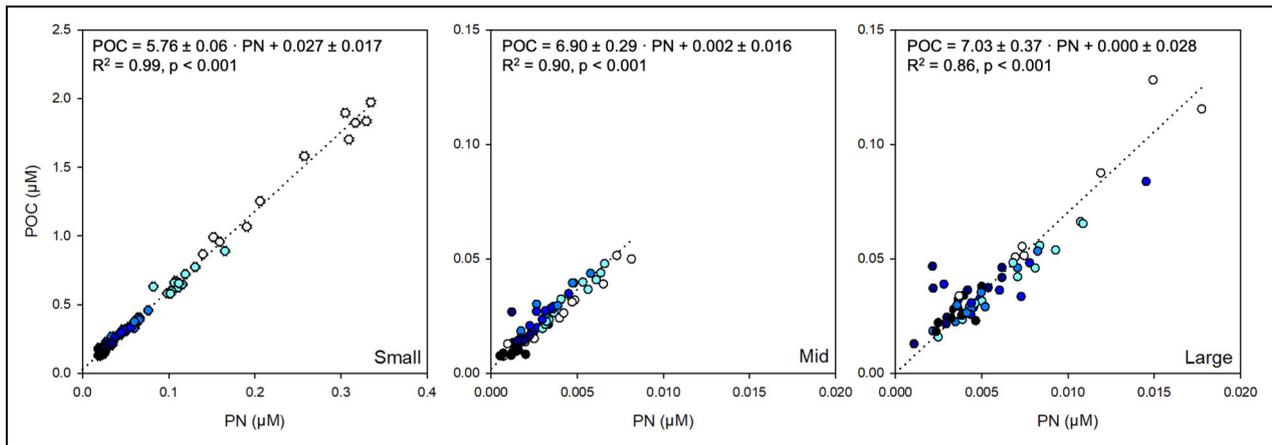
Figure 5. Relationship between particulate organic carbon (POC) and particulate nitrogen (PN) in size-fractionated particles. POC versus PN for small (1–5 μm), midsized (5–51 μm), and large (>51 μm) particles combining all pump casts and depths (50–500 m). Note the different scales on both axes between small versus midsized and large particles. Colors show different depths, with lighter colors indicative of shallower waters and darker colors of deeper waters. The dotted line shows the mean POC/PN ratio computed by type-II linear regression for each size fraction. DOI: https://doi.org/10.1525/elementa.2020.00166.f5

at 50 m (0.49 ± 0.12 dpm L^{-1} and 0.030 ± 0.018 dpm L^{-1}, respectively, $n = 11$ each) before decreasing by a factor of 2 to relatively constant activities between 100 and 500 m. In contrast, in midsized particles, ^{234}Th activities increased from 50 to 150 m (0.027 ± 0.010 dpm L^{-1}, $n = 12$), before declining in deeper waters (**Figure 2**).

3.2. Molar ratios in size-fractionated particles
Elemental molar ratios for each particle size class were determined by the arithmetic mean ($\pm$standard deviation) at each depth horizon combining all pump casts. In cases of a strong correlation ($R^2 > 0.60$), mean molar ratios were also determined by the slope ($\pm$standard deviation) of type-II linear regressions obtained for each pair of elements either at a specific depth horizon or by combining different depths. For easier comparison with previous studies, we hereafter use POC in the numerator for POC/PN, POC/TPP (e.g., Martiny et al., 2014), and POC in the denominator for bSi/POC and PIC/POC (e.g., Timothy et al., 2013).

Mean POC/PN ratios were lower in small particles (6.0 ± 0.3 to 6.9 ± 0.6, $n = 11$, for each depth), followed by large particles (6.3 ± 0.4 to 10.5 ± 5.0, $n = 10$–12) and midsized particles (7.1 ± 0.5 to 9.5 ± 4.4, $n = 11$–12) with no clear trends with depth for any particle size class (**Figure 4**). POC was strongly correlated to PN in all particle size classes across all depths (**Figure 5**). The slopes were 5.76 ± 0.06 for small, 6.90 ± 0.29 for midsized, and 7.03 ± 0.37 for large particles. A positive intercept was obtained for small particles, unlike for midsized and large particles.

Ratios of POC/TPP in small and large particles did not show a clear trend with depth, with mean ratios of 118 ± 32 ($n = 58$) and 175 ± 100 ($n = 15$), respectively, when combining all data (**Figure 4**). Ratios of POC/TPP in midsized particles were below the Redfield ratio (106) in shallow waters with a mean ratio of only 26 ± 9 ($n = 3$) at 50 m, which increased with depth to 152 ± 35 ($n = 2$) at 330

m, indicating stronger TPP attenuation relative to POC. POC was strongly correlated with TPP only in small particles combining all depths (slope = 132 ± 6, $R^2 = 0.88$, $P < 0.001$).

Mean bSi/POC ratios were lower in the small size class (0.03 ± 0.02 to 0.16 ± 0.07, $n = 11$ for each depth) relative to midsized (0.16 ± 0.04 to 0.94 ± 0.26, $n = 11$–12) and large (0.34 ± 0.09 to 0.48 ± 0.14, $n = 12$) particles in the upper 500 m (**Figure 4**). Interestingly, bSi/POC ratios increased with depth in small and midsized particles, while they did not show a trend with depth in large particles. In small particles, bSi/POC ratios increased by a factor of 4 between 50 and 500 m, indicating stronger attenuation of POC relative to bSi. In midsized particles, the bSi/POC ratios increased by a factor of 6 over this depth range due to an increase in bSi concurrent with a decrease in POC. bSi was correlated to POC in large particles combining all depths (slope = 0.50 ± 0.04, $R^2 = 0.70$, $P < 0.001$) and midsized particles only for data from 50 m (slope = 0.10 ± 0.01, $R^2 = 0.82$, $P < 0.001$). Weak or nonsignificant correlations between bSi and POC were found for small particles and midsized particles below 50 m.

Mean PIC/POC ratios were more variable in small particles (0.003 ± 0.002 to 0.09 ± 0.03, $n = 7$–11 for each depth) than in midsized and large particles (**Figure 4**). In small particles, PIC/POC ratios increased by an order of magnitude from 50–100 m to 330–500 m driven by POC attenuation. In contrast, PIC/POC ratios in midsized and large particles showed no clear trend with depth and were comparable (Mann–Whitney rank-sum test, $P = 0.618$). PIC was correlated to POC in large particles combining all depths (slope = 0.052 ± 0.006, $R^2 = 0.69$, $P < 0.001$).

3.3. Ratios between bioelements and ^{234}Th in size-fractionated particles
The determination of element to ^{234}Th ratios (hereafter referred to as element/Th) on particles is fundamental for

Table 2. Cruise-average element/^{234}Th ratios.[a] DOI: https://doi.org/10.1525/elementa.2020.00166.t2

| Depth (m) | PN/^{234}Th (µmol dpm^{-1}) | | | | | | bSi/^{234}Th (µmol dpm^{-1}) | | | | | |
| | 1−5 µm | | 5−51 µm | | >51 µm | | 1−5 µm | | 5−51 µm | | >51 µm | |
	Average	SD	Average	SD	Average	SD	Average	SD	Average	SD	Average	SD
50	0.50	0.08	0.80	0.36	0.29	0.08	0.10	0.05	0.78	0.24	0.89	0.38
65	*0.49*	*0.08*	*0.63*	*0.23*	*0.30*	*0.08*	*0.10*	*0.05*	*0.72*	*0.21*	*0.83*	*0.33*
80	*0.49*	*0.08*	*0.46*	*0.13*	*0.32*	*0.08*	*0.11*	*0.06*	*0.67*	*0.18*	*0.78*	*0.28*
100	0.48	0.08	0.23	0.04	0.34	0.08	0.12	0.06	0.59	0.15	0.71	0.21
120	*0.41*	*0.08*	*0.18*	*0.03*	*0.32*	*0.09*	*0.12*	*0.07*	*0.56*	*0.17*	*0.72*	*0.23*
150	0.30	0.06	0.12	0.03	0.28	0.09	0.11	0.07	0.53	0.19	0.74	0.25
200	0.20	0.04	0.13	0.02	0.34	0.11	0.11	0.06	0.53	0.20	0.80	0.34
280	*0.16*	*0.02*	*0.13*	*0.03*	*0.29*	*0.13*	*0.13*	*0.07*	*0.53*	*0.19*	*0.78*	*0.32*
330	0.13	0.02	0.11	0.03	0.27	0.13	0.14	0.07	0.52	0.19	0.77	0.30
500	0.13	0.02	0.12	0.05	0.27	0.09	0.10	0.05	0.80	0.18	0.86	0.33
	TPP/^{234}Th (µmol dpm^{-1})						PIC/^{234}Th (µmol dpm^{-1})[b]					
50	0.023	0.006	0.184	0.077	0.014	0.003	0.035	0.028	0.058	0.019	0.074	0.050
65	*0.022*	*0.005*	*0.137*	*0.048*	*0.015*	*0.004*	–	–	–	–	–	–
80	*0.022*	*0.004*	*0.089*	*0.025*	*0.015*	*0.004*	–	–	–	–	–	–
100	0.022	0.003	0.024	0.004	0.017	0.005	0.009	0.005	LOD	–	0.032	0.016
120	*0.021*	*0.006*	*0.016*	*0.004*	*0.017*	*0.006*	–	–	–	–	–	–
150	0.020	0.010	0.009	0.003	0.017	0.007	0.040	0.009	LOD	–	0.037	0.016
200	0.012	0.002	0.009	0.002	0.012	0.001	0.064	0.012	0.010	0.002	0.046	0.022
280	*0.009*	*0.002*	*0.007*	*0.001*	*0.009*	*0.001*	–	–	–	–	–	–
330	0.008	0.002	0.007	0.000	0.008	0.001	0.079	0.022	LOD	–	0.056	0.043
500	0.010	0.001	0.008	0.001	0.013	0.011	0.062	0.016	0.031	0.006	0.055	0.018

LOD = limit of detection; ^{234}Th = thorium-234; PN = particulate nitrogen; bSi = biogenic silica; TPP = total particulate phosphorus; PIC = particulate inorganic carbon.

[a]Element/^{234}Th ratios for size-fractionated particles were measured at 50, 100, 150, 200, 330, and 500 m. Average ratios at these depths were obtained from the arithmetic mean ($\pm$ standard deviation). Values shown in italics are interpolated linearly.

[b]PIC/^{234}Th ratios in midsized particles at 50 and 200 m represent just one station (others were below the LOD), where the uncertainty was obtained by propagating the uncertainties of the PIC and ^{234}Th measurements.

estimating particulate export fluxes of any element by using the ^{234}Th proxy (Buesseler et al., 2006). In this study, cruise-average element/Th ratios were determined at each sampled depth from the arithmetic mean ($\pm$ standard deviation) of the ratios in each particle size class by combining all pump casts (**Table 2**), following the same method detailed in Buesseler et al. (2020a) for POC/Th ratios.

Ratios of PN/Th showed a decrease with depth in small and midsized particles but did not significantly change with depth in large particles, exhibiting the same trends as POC/Th ratios (**Figure 6**). In small particles, the mean PN/Th ratios were 0.48–0.50 µmol dpm^{-1} ($n = 11$–12 each) at 50–100 m decreasing to 0.13 $\pm$ 0.02 µmol dpm^{-1} ($n = 11$–12 each) by 330–500 m. Additional samples collected in the mixed layer (20 m) had the highest

ratios (0.64 $\pm$ 0.02 µmol dpm^{-1}, $n = 2$; **Figure 6**). In midsized particles, PN/Th ratios decreased steeply from 50 m (0.80 $\pm$ 0.36 µmol dpm^{-1}, $n = 11$) to 150–500 m (0.11–0.13 µmol dpm^{-1}, $n = 9$–11 each). Ratios of PN/Th in large particles were on average 0.30 $\pm$ 0.10 µmol dpm^{-1} ($n = 58$) combining all depths. The lack of a decrease in POC/Th and PN/Th ratios in large particles with depth is likely due to the presence of zooplankton swimmers that could not be easily removed from the filters (see details in Buesseler et al., 2020a).

Ratios of TPP/Th also decreased with depth in small and midsized particles but remained constant throughout the water column in the largest size class (**Figure 6**). Ratios of TPP/Th in small particles decreased by a factor of 2 from 50–150 m (means of 0.020–0.023 µmol dpm^{-1}, $n = 11$ for each depth) to 330–500 m. Ratios of TPP/Th in
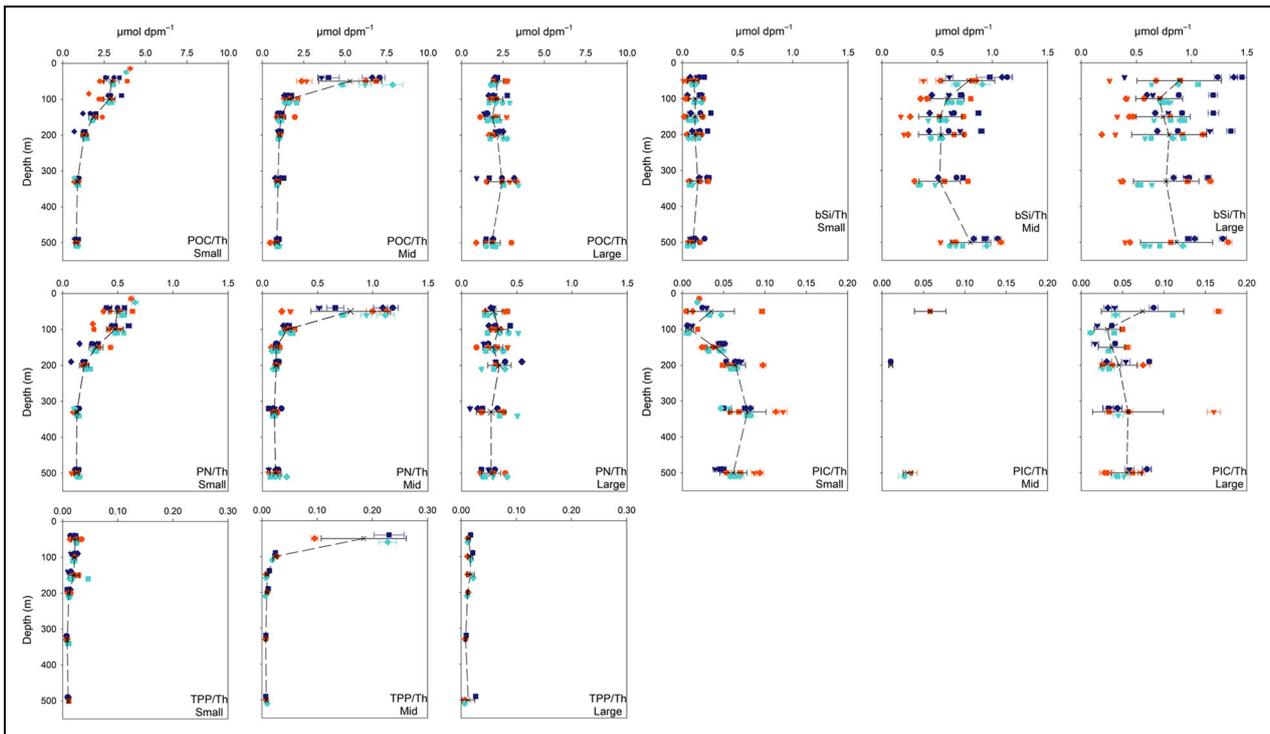
Figure 6. Size-fractionated element/thorium-234 (^{234}Th) ratios versus depth. Ratios of particulate organic carbon (POC)/^{234}Th, particulate nitrogen (PN)/^{234}Th, total particulate phosphorus (TPP)/^{234}Th, biogenic silica (bSi)/^{234}Th, and particulate inorganic carbon (PIC)/^{234}Th in small (1–5 μm), midsized (5–51 μm), and large (>51 μm) particles. Each symbol represents a specific in situ pump cast color-coded by sampling "epoch" (Epoch 1 = dark blue, Epoch 2 = red, and Epoch 3 = turquoise), as in **Figure 1**. Error bars were obtained by propagating the uncertainties of ^{234}Th and the bioelement considered for each element/^{234}Th ratio. Black crosses show average ($\pm$standard deviation) element/^{234}Th ratios. Ratios of POC/^{234}Th from Buesseler et al. (2020a) are shown for comparison. DOI: https://doi.org/10.1525/elementa.2020.00166.f6

midsized particles at 50 m (0.184 $\pm$ 0.077 μmol dpm^{-1}, $n = 3$) were an order of magnitude higher than in deeper waters. In large particles, TPP/Th ratios averaged 0.014 $\pm$ 0.006 μmol dpm^{-1} ($n = 15$) combining all depths. Below 50 m, TPP/Th ratios were comparable across the three particle size classes (Kruskal-Wallis ANOVA on ranks, $P = 0.120$).

Ratios of bSi/Th were constant with depth in all particle classes, with the exception of higher bSi/Th ratios found at 50 and 500 m in midsized particles (one-way ANOVA, $P \leq 0.001$; **Figure 6**). We therefore computed depth-averaged bSi/Th ratios and compared them by epoch and particle class to sediment trap material (Estapa et al., 2021; **Figure 7**). Ratios of bSi/Th in size-fractionated particles in Epoch 1 were higher than in Epochs 2 and 3 by 30%–50%, a temporal trend not supported by trap data. The mean bSi/Th ratio in small particles (0.11 $\pm$ 0.06 μmol dpm^{-1}, $n = 70$) was 5 to 7 times lower than in midsized and large particles (0.63 $\pm$ 0.22 and 0.79 $\pm$ 0.30 μmol dpm^{-1}, respectively, $n = 70$ each). Ratios of bSi/Th in midsized particles were not significantly different than those found in trap material (0.59 $\pm$ 0.22 μmol dpm^{-1}, $n = 32$; t test, $P = 0.867$; **Figure 7**).

Ratios of PIC/Th were highly variable, peaking at 50 m for large particles and between 200 and 500 m for small particles (**Figure 6**). Combining all data, PIC/Th ratios

were not significantly different across size classes (Kruskal–Wallis ANOVA on ranks, $P = 0.253$; Figure S2), averaging 0.052 $\pm$ 0.027 μmol dpm^{-1} ($n = 62$) in small, 0.033 $\pm$ 0.020 μmol dpm^{-1} ($n = 4$) in midsized, and 0.052 $\pm$ 0.032 μmol dpm^{-1} ($n = 42$) in large particles.

In addition to bSi, PN, TPP and PIC were measured in trap material. However, as discussed in Estapa et al. (2021), many of the measurements were affected substantially by swimmer contamination. A small subset of samples ($n = 7$) covering depths from 100 to 500 m were considered to be uncontaminated and were characterized by median ratios of 0.37 μmol dpm^{-1} for PN/Th, 0.007 μmol dpm^{-1} for TPP/Th, and 0.080 μmol dpm^{-1} for PIC/Th (Estapa et al., 2021). Trap PN/Th and PIC/Th ratios were within the range of those measured in size-fractionated particles, but TPP/Th ratios tended to be lower, consistent with possible solubilization of TPP in trap samples (Antia, 2005; Buesseler et al., 2007b; Estapa et al., 2021).

3.4. Fluxes of major bioelements derived from ^{234}Th
In this study, we calculated cruise-average export fluxes of PN, TPP, bSi, and PIC following the same approach presented in Buesseler et al. (2020a) for POC flux. The fluxes of these bioelements were determined from the ^{234}Th fluxes estimated using an average of the steady-state and non-steady-state models based on numerous ^{234}Th
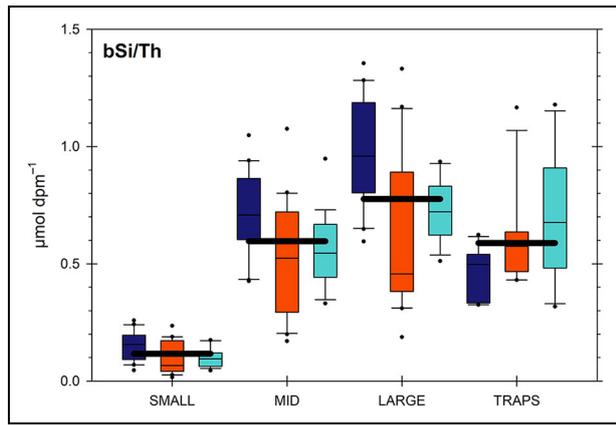
Figure 7. Biogenic silica (bSi)/thorium-234 (^{234}Th) ratios in different particle classes. Ratios of bSi/^{234}Th in small (1–5 μm), midsized (5–51 μm), large (>51 μm), and sediment trap (Estapa et al., 2021) particles combining samples from 100 to 500 m. Colors represent sampling "epochs" (Epoch 1 = dark blue, Epoch 2 = red, and Epoch 3 = turquoise), as in **Figure 1**. The thick black lines show the cruise-average bSi/^{234}Th ratios for each particle class. The base of the boxes indicates the 25th percentile, the line within the boxes marks the median, and the top of the boxes indicates the 75th percentile. Error bars above and below the boxes indicate the 90th and 10th percentiles. Black dots show the data points outside the 10th–90th percentile range. DOI: https://doi.org/10.1525/elementa.2020.00166.f7

measurements (see Buesseler et al., 2020a, for details) and the element/Th ratios measured in midsized particles (usually from $n = 12$ measurements at each depth for PN and bSi, $n = 3$ for TPP, and a single mean for all particle size classes and depths for PIC based on $n = 108$ measurements, see below). These results are presented in **Table 3** and **Figure 8**. In addition, fluxes measured at each individual station sampled during the cruise are given in Table S3.

In using midsized particle ratios to convert ^{234}Th fluxes to bioelement fluxes, we assumed that this particle size class represented the composition of sinking material at Station P. This assumption is based on several reasons. First, ratios of POC/Th, PN/Th, and TPP/Th in midsized particles decreased with depth (**Figure 6**). A decreasing trend is typically reported in ^{234}Th studies and is hypothesized to be due to the preferential remineralization of major bioelements relative to ^{234}Th and continued ^{234}Th scavenging as particles sink (Buesseler et al., 2006; Puigcorbé et al., 2020). Second, visual inspection of the >51 μm pore-size filters and the absence of a decrease in POC/Th, PN/Th, and TPP/Th ratios with depth in large particles (**Figure 6**) suggests zooplankton contamination (Buesseler et al., 2020a). Third, the agreement between POC fluxes measured by sediment traps after swimmer correction and those modeled from microscopic analyses of sinking particles collected in polyacrylamide gel traps that exclude our small size fraction (Estapa et al., 2021) suggests a minor contribution of small particles to sinking particle

fluxes during EXPORTS. Finally, the agreement between the bSi/Th ratios in midsized particles and trap material (**Figure 7**) supports that midsized particles were representative of sinking particle composition.

In order to estimate sinking fluxes of PIC, we used the mean PIC/Th ratio obtained by combining all depths and particle size classes (0.045 $\pm$ 0.016 μmol dpm^{-1}). This approach was used because most of the PIC measured in midsized particles fell below the limit of detection and PIC/Th ratios were not significantly different across size classes (Figure S2). PIC fluxes should therefore be considered upper estimates.

Cruise-average PN and TPP fluxes were highest at 50 m and decreased sharply by a factor of 4 and 10, respectively, to 0.22 $\pm$ 0.07 mmol N m^{-2} d^{-1} and 0.019 $\pm$ 0.007 mmol P m^{-2} d^{-1} at the base of the euphotic zone at 120 m (**Figure 8**). Below this depth horizon, PN and TPP fluxes were constant. The POC flux profile showed a similar vertical distribution to PN and TPP fluxes but decreased by a factor of 3 from 50 to 120 m (Buesseler et al., 2020a; **Figure 8**). Fluxes of bSi and PIC varied to a much lesser extent, ranging from 0.55 $\pm$ 0.40 to 1.06 $\pm$ 1.09 mmol Si m^{-2} d^{-1} and from 0.047 $\pm$ 0.015 to 0.062 $\pm$ 0.051 mmol C m^{-2} d^{-1} over the depth range sampled; indeed, these fluxes were the same within uncertainties across all depths (**Figure 8**).

4. Discussion

4.1. Profiles of major bioelements and ^{234}Th in size-fractionated particles

4.1.1. Particle concentrations from in situ pumps

In this study, we distinguish three distinct patterns in the vertical profiles of size-fractionated particles (**Figures 2** and **3**). First, the profiles of POC, PN, bSi, and ^{234}Th are characterized by a decrease in concentrations in small and large particles from 50 to 150 m and constant or increasing concentrations in midsized particles. Below 150 m, POC, PN, bSi, and ^{234}Th concentrations remained relatively constant or slightly decreased in all particle sizes. Second, TPP concentrations decreased from 50 to 150 m in small and midsized particles and remained relatively constant at deeper depths. Large particles, however, showed similar TPP concentrations throughout the upper 500 m. Lastly, the PIC profiles in small particles showed peak concentrations at 50 m and in deep waters between 200 and 500 m.

Decreases in POC, PN, bSi, and ^{234}Th concentrations in small and large particles within the euphotic zone and the upper twilight zone are consistent with particle consumption and disaggregation (Ploug et al., 1999; Kiørboe, 2000; Lam and Marchal, 2015). The largest concentration decrease was observed for POC and PN in small particles from 50 to 150 m, which is 2 times greater than for bSi and ^{234}Th over the same depth range and particle size. This strong decrease indicates a preferential consumption of particulate organic matter by bacterial remineralization and zooplankton grazing (Ragueneau et al., 2002; Buesseler et al., 2006). Interestingly, concentrations in midsized particles did not decrease between 50 and 150 m and, in fact, bSi and ^{234}Th increased. The concurrent loss of bSi and ^{234}Th in small and large particles suggests that the

Table 3. Cruise-average ^{234}Th, POC, PN, TPP, bSi and PIC fluxes. DOI: https://doi.org/10.1525/elementa.2020.00166.t3

Depth (m)	^{234}Th Flux (dpm m^{-2} d^{-1})[a]		POC Flux (mmol C m^{-2} d^{-1})[a]		PN Flux (mmol N m^{-2} d^{-1})[b]		TPP Flux (mmol P m^{-2} d^{-1})[b]		bSi Flux (mmol Si m^{-2} d^{-1})[b]		PIC Flux (mmol C m^{-2} d^{-1})[c]	
	Average	Uncert.	Average	Uncert.	Average	Uncert.	Average	Uncert.	Average	Uncert.	Average	Uncert.
50	1,033	184	5.5	1.7	0.82	0.31	0.191	0.067	0.81	0.23	0.047	0.015
65	1,157	231	4.9	1.4	0.73	0.24	0.159	0.051	0.84	0.24	0.052	0.017
80	1,220	273	3.8	1.1	0.56	0.17	0.109	0.033	0.81	0.24	0.055	0.019
100	1,238	312	2.0	0.6	0.28	0.08	0.029	0.008	0.73	0.23	0.056	0.020
120	1,227	383	1.7	0.6	0.22	0.07	0.019	0.007	0.69	0.26	0.055	0.022
150	1,163	479	1.3	0.6	0.14	0.06	0.011	0.005	0.61	0.30	0.053	0.026
200	1,029	696	1.1	0.7	0.13	0.09	0.009	0.007	0.55	0.40	0.047	0.034
280	1,146	726	1.1	0.7	0.15	0.09	0.008	0.005	0.60	0.41	0.052	0.035
330	1,367	1,076	1.3	1.0	0.15	0.12	0.010	0.008	0.71	0.59	0.062	0.051
500	1,322	1,341	1.2	1.2	0.16	0.17	0.011	0.011	1.06	1.09	0.060	0.063

^{234}Th = thorium-234; POC = particulate organic carbon; PN = particulate nitrogen; TPP = total particulate phosphorus; bSi = biogenic silica; PIC = particulate inorganic carbon.

[a]Cruise-average ^{234}Th and POC fluxes at Station P during the EXport Processes in the Ocean from RemoTe Sensing field campaign as reported by Buesseler et al. (2020a). POC fluxes were calculated by using the ^{234}Th fluxes and POC/^{234}Th ratios in midsized particles collected using in situ pumps.

[b]PN, TPP, and bSi fluxes were calculated by using the corresponding element/^{234}Th ratio in midsized particles (**Table 2**) and the cruise-average ^{234}Th fluxes. Uncertainties were calculated by propagating the uncertainties from the steady-state and non-steady-state flux estimates as detailed in Buesseler et al. (2020a) for POC flux.

[c]PIC fluxes were calculated as PN, TPP, and bSi except that a single value of PIC/^{234}Th was used combining all particle size classes and depths (**Table 2**; see details in Section 3.4).

midsized particle pool was sustained by aggregation of small particles and/or disaggregation of large particles. However, the lower POC/TPP ratios in midsized particles compared to small and large particles at 100 m (**Figure 4**) suggest that there was also in situ production of midsized particles with low POC/TPP ratios in the lower euphotic zone (e.g., dinoflagellates or diatoms; see Section 4.2).

TPP concentrations in small particles decreased in a similar manner to POC and PN between 50 and 150 m, although at some stations, the decrease was less pronounced for TPP. In contrast to POC and PN, the steep decrease in TPP in midsized particles between 50 and 150 m (factor of 5) suggests preferential attenuation of TPP at these depths for this size class. In large particles, relatively invariant TPP concentrations and high POC/TPP ratios throughout 50–500 m (**Figures 2** and **4**) may be the result of enhanced remineralization of TPP in the upper euphotic zone.

Small particle PIC concentrations exhibit a distinct profile, with minimum concentrations at 100 m and maximum concentrations at 50 m and between 200 and 500 m. This pattern is of interest as the calcite saturation horizon around Station P lies between 250 and 500 m, while aragonite, a minor component of PIC in the NE Pacific subarctic gyre, becomes undersaturated at 100–200 m (Feely et al., 2002; Dong et al., 2019). PIC concentrations in midsized and large particles were low throughout the upper 500 m (**Figure 3**), suggesting that disaggregation

cannot explain the increase in PIC concentrations measured at depth in small particles. One explanation could be the production of fecal pellets by vertically migrating zooplankton that feed in surface waters at night and migrate to depth during the day (Steinberg and Landry, 2017). Other EXPORTS data sets show evidence of coccolithophores in both shallow and deep waters near Station P, including the microscopic identification of individual coccolithophore cells in gel traps between 100 and 500 m (Bodel et al., 2020).

4.1.2. Comparison of pump-derived POC, PN, and bSi concentrations with other EXPORTS data sets

Size-fractionated POC and PN concentrations in the upper 70 m of the water column were also determined from the R/V *Roger Revelle* using Niskin bottles. This data set shows that at 50 m 21% of POC and 24% of PN were in the >5 μm size fraction ($n = 3$; A Marchetti, personal communication, October 2020). In contrast, only 6% of the pump POC and PN was measured in this size fraction at the same depth. The difference between bottles and pumps across size classes may be due to multiple factors. First, bottle size-fractionated POC and PN were obtained from 24-h incubations to determine ^{13}C uptake rates. As such, samples were not filtered immediately after collection and may have been altered by time and handling (e.g., aggregation). Also, in situ pump sampling was conducted on the R/V *Sally Ride*, which covered a larger spatial scale and
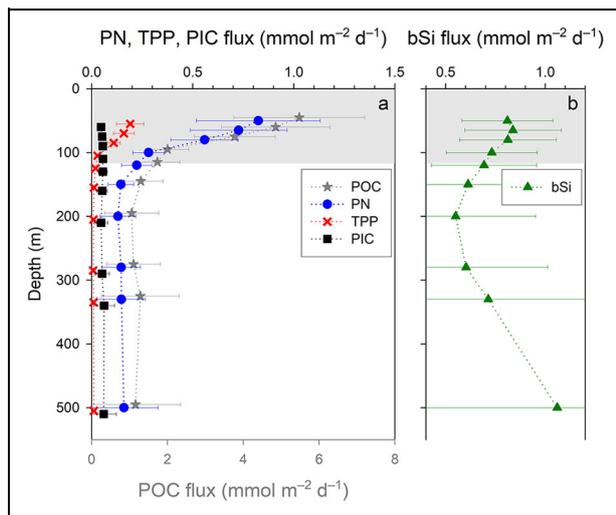
Figure 8. Cruise-average sinking fluxes of major bioelements versus depth. Cruise-average fluxes of (a) particulate organic carbon (gray; Buesseler et al., 2020a), particulate nitrogen (blue), total particulate phosphorus (red), and particulate inorganic carbon (black) and (b) biogenic silica (green), all estimated using the thorium-234 proxy and in situ pumps (see Section 3.4). The gray-shaded area shows the euphotic zone defined by the primary production zone (117 ± 5 m) and 0.1% photosynthetic active radiation (118 ± 9 m). Fluxes for each element are offset by 5 m to facilitate visualization. Note different scales on the x-axes. DOI: https://doi.org/10.1525/elementa.2020.00166.f8

a wider range of conditions compared to the sampling conducted on the R/V *Roger Revelle* (Siegel et al., 2021). Moreover, lower pump POC and PN concentrations in the larger size fractions may reflect particle loss from the Nitex screens during pumping by means of disaggregation or breakage of fragile particles, and/or inefficient rinsing of the Nitex screens. Maiti et al. (2012) showed that [234]Th activity in large particles decreases with increasing pump flow rate (2–9 L min^{−1}) with varying intensity depending on the site. As such, >5 µm particles would have been collected on the QMA filters and classified as small particles. Buesseler et al. (1998) further found that up to 20% of particulate [234]Th may remain on the Nitex screens after rinsing. However, even assuming a loss of 20% of POC and PN in the midsized and large fractions, the discrepancy between bottle and pump results would still remain. The concentrations of POC and PN obtained using Niskin bottles and in situ pumps during EXPORTS will be compared in detail elsewhere.

bSi concentrations can also be compared to those obtained in the upper 70 m from Niskin bottles on the R/V *Roger Revelle*. Average total bSi concentrations at 50 m from bottles (0.08 ± 0.03 µM, $n = 3$; M Brzezinski, personal communication, October 2020) agree with the concentrations measured with pumps (0.08 ± 0.04 µM, $n = 11$). However, size-fractionated bottle data show that 69% of bSi was on the >5 µm size fraction at this depth (M Brzezinski, personal communication, October 2020),

compared to 39% based on pump samples despite the agreement in total bSi. To some extent, bSi concentrations in our midsized and large fractions may be underestimated and concentrations in small particles overestimated if vertically oriented and elongated diatoms passed through the Nitex screens during filtration. Indeed, amplicon sequencing data show that sequences encoded by *Pseudo-nitzschia* (pennate), followed by *Thalassiosira* (centric) and *Fragilariopsis* (pennate), were relatively abundant in the amplified sequences from the euphotic zone diatom community, accounting together for >70% of the sequences (S Lerch, personal communication, February 2021). Indeed, the needle-shaped *Pseudo-nitzschia* were found to have widths smaller than 5 µm and form chains longer than 51 µm (H. Sosik, personal communication, February 2021). Alternatively, the disruption of diatom chains (such as *Pseudo-nitzschia*) during pump filtration could have resulted in the release of single diatom cells relative to bottle filtration. In fact, fucoxanthin to total chlorophyll-*a* ratios obtained by high-performance liquid chromatography from R/V *Sally Ride* bottle and QMA pump samples are very similar (e.g., at 50 m: 0.157 ± 0.018, $n = 38$, for bottles; 0.147 ± 0.007, $n = 11$, for pumps; DOI: 10.5067/SeaBASS/EXPORTS/DATA001), yet bottle samples should represent all size classes while pump samples should only represent a subfraction (1–5 µm). This similarity suggests that >5 µm diatoms may have passed through the Nitex screens leading to an overestimation of bSi concentrations in small particles using in situ pumps.

Taken together, we acknowledge that size-fractionated POC, PN, and bSi bottle data from the R/V *Roger Revelle* suggest that large volume filtration may have resulted in lower POC, PN, and bSi concentrations in midsized and large particles and higher bSi concentrations in small particles. In contrast to bSi, the lower concentrations of POC and PN in midsized and large particles suggest that these effects would not result in significant overestimates in the small size class. We found no evidence that under- or overestimates in concentrations occurred below the shallowest in situ pump at 50 m. Furthermore, molar and element/Th ratios are not impacted in the same way as concentrations. The loss of material from a given size class would only change a given ratio if the amount of material lost was significant and characterized by a different composition relative to the bulk material. Likewise, the gain of material to a given size class would only affect the ratio if the amount of material added was significant and possessed a different composition relative to the bulk. Future experiments involving collocated measurements in bottle and in situ pump samples will be needed, ideally using the same filters and similar sample handling procedures.

4.2. Molar ratios in size-fractionated particles
Molar ratios of POC/PN from in situ pump filtration during EXPORTS were relatively close to the Redfield ratio (6.6) and in agreement with previous observations at Station P. Specifically, mean POC/PN ratios were 6.4 ± 0.8 ($n = 70$) in small, 8.2 ± 2.6 ($n = 64$) in midsized, and 7.6 ± 2.7 ($n = 58$) in large particles. These POC/PN ratios are

comparable to those measured in sediment trap samples collected during EXPORTS at depths from 100 to 500 m (median: 7.0, $n = 7$; Estapa et al., 2021). Ratios of POC/PN on suspended matter collected at Station P from 50–500 m in August 1996 (6.7 $\pm$ 1.2, $n = 31$) are within the range of EXPORTS observations, but literature values from September show much higher variability (Martiny et al., 2014). Other studies using moored sediment traps at Station P have reported POC/PN ratios of 13 at 200 m during the same season, but these elevated ratios were attributed to lipid accumulation by <1,000 μm swimmers that were not removed from trap samples (Timothy et al., 2013). High POC/PN ratios obtained from time-series measurements of surface-tethered traps were also hypothesized to be affected by swimmers that passed through the 500 or 1,000 μm screens used to separate swimmers from samples (Wong et al., 2002).

Another way to examine POC/PN ratios is from POC versus PN relationships. In this study, POC was strongly correlated to PN in each size fraction (**Figure 5**). Previous work has used the slope of such relationships to determine remineralization or particle degradation ratios based on sinking (Lamborg et al., 2008) and suspended (Lam et al., 2018) particles. Here, we identified a lower POC/PN slope in small particles compared to the mean POC/PN (5.8 vs. 6.4; *t* test, $P < 0.001$) and a small positive intercept (PN = 0 and POC = 0.027 $\pm$ 0.017 μM). These results suggest the existence of a POC component that does not degrade over the 50–500 m range. The POC/PN slope is also lower in midsized particles compared to the mean, but in large particles, POC/PN ratios obtained from both methods (**Figures 4** and **5**) are comparable (midsized: 6.9 vs. 8.2, *t* test, $P < 0.001$; large: 7.0 vs. 7.6, *t* test, $P = 0.131$). The lack of a significant intercept in midsized particles (PN = 0 and POC = 0.002 $\pm$ 0.016 μM) suggests that the lower POC/PN from the slope is likely due to higher variability in POC/PN ratios. Combined, these results suggest that POC and PN have similar remineralization length scales in all size classes, resulting in invariant POC/PN ratios in the upper 500 m (**Figure 4**). Similar conclusions were drawn by Lamborg et al. (2008) and Lam et al. (2018). They are also consistent with the findings by Wong et al. (2002) who determined a remineralization ratio close to the Redfield ratio by using three independent methods and data from the upper 1,000 m of the water column at Station P.

Ratios of POC/TPP in small and large particles showed no clear trends with depth, with mean ratios of 118 $\pm$ 32 and 175 $\pm$ 100, respectively (**Figure 4**). In contrast, POC/TPP ratios in midsized particles were very low (17–35) at 50 m, which may reflect the elemental stoichiometry of the plankton community. During EXPORTS, the 5–51 μm phytoplankton carbon biomass at 50 m was dominated by dinoflagellates with a small fraction comprised of diatoms (approximately 30% vs. <10%; H. Sosik, personal communication, November 2020) consistent with low bSi concentrations (**Figure 2**). Both dinoflagellates and diatoms may exhibit low POC/TPP ratios due to reduced cell wall material or to accumulation of inorganic phosphorus compounds, such as polyphosphate (Twining et al., 2004;

Price, 2005; Martiny et al., 2013; Lomas et al., 2019; Zhang et al., 2019). Below 50 m, POC/TPP ratios in midsized particles (109 $\pm$ 35, $n = 14$) were more similar to the other size classes and close to those reported for suspended organic matter from the upper 300 m in the Pacific subarctic region (Teng et al., 2014). The POC/TPP ratios measured in sediment traps during EXPORTS (median: 264, $n = 7$; Estapa et al., 2021) are substantially higher than those determined by in situ filtration, potentially due to solubilization of TPP in traps prior to sample processing (Antia, 2005; Buesseler et al., 2007b; Estapa et al., 2021).

Ratios of bSi/POC were consistently higher in midsized and large particles compared to small particles, suggesting a larger contribution of siliceous plankton to the larger particle pools and/or a different degree of diatom silicification between size classes. The average bSi/POC ratios measured in >5 μm particles were on average 0.4–0.5, but at 50 m, ratios were significantly lower for midsized particles compared to large particles (0.16 $\pm$ 0.04 vs. 0.41 $\pm$ 0.21, respectively). The bSi/POC ratio measured in large particles is 3 times higher than that typical of diatom cultures growing under nutrient-replete conditions (0.13; Brzezinski, 1985). Low levels of iron affect the elemental stoichiometry of diatoms leading to an increase in their cellular bSi/POC and bSi/PN ratios (Hutchins and Bruland, 1998; Firme et al., 2003; Marchetti and Cassar, 2009). Given that large phytoplankton at Station P are iron-limited (Harrison, 2002), these high bSi/POC ratios may reflect a significant contribution of iron-stressed diatoms to the >51 μm particle pool in the euphotic zone. The bSi/POC ratio determined from the correlation between bSi and POC fluxes measured with sediment traps during EXPORTS (0.29 $\pm$ 0.02; Estapa et al., 2021) falls between that measured in the small and larger size fractions. Furthermore, the average bSi/POC ratios measured using moored sediment traps at 200 m at Station P in summer and the fall from 1989 to 2006 (0.46–0.55; Timothy et al., 2013) are similar to those presented here for midsized and large particles.

Another important finding is that bSi/POC ratios in small and midsized particles clearly increased with depth (**Figure 4**), providing evidence of heterotrophic consumption of organic matter as these smaller particles sink through the water column. In contrast, bSi/POC ratios in large particles remained relatively constant with depth. This finding suggests that large, ballasted particles escape POC loss due to rapid sinking (Armstrong et al., 2002; Klaas and Archer, 2002; De La Rocha and Passow, 2007; Honjo et al., 2008). Indeed, gel traps collected a large number of heavily silicified diatoms that sank as individual cells or in chains, predominantly composed of *Fragilariopsis*-like cells which spanned sizes from 43 to 107 μm (Bodel et al., 2020). However, high and invariant POC/Th ratios with depth in large particles (**Figure 6**) and visual analysis of the >51 μm filters suggested contamination by C-rich swimmers especially in the deeper samples (Buesseler et al., 2020a). The presence of swimmers may therefore partially explain the lack of bSi/POC vertical change in this size class. Furthermore, large Rhizaria with siliceous

tests, which were identified in the gel traps (Bodel et al., 2020), could have also affected bSi/POC ratios in large particles.

Ratios of PIC/POC in small particles increased from the base of the euphotic zone up to 0.08–0.09 at 330–500 m (**Figure 4**) reflecting a more rapid loss of POC relative to calcium carbonate. In contrast, PIC/POC ratios in midsized and large particles did not show a clear trend with depth and remained at very low values throughout the upper 500 m (0.026 ± 0.014). The PIC/POC ratios measured in the larger size fractions are in good agreement with those measured in sediment trap material during EXPORTS (median: 0.035, $n = 7$; Estapa et al., 2021). Compared to previous studies, PIC/POC ratios obtained from size-fractionated particles are consistent with those measured in sediment trap material collected over the 150–500 m depth range in the NW Pacific subarctic gyre (Lamborg et al., 2008). However, much higher PIC/POC ratios have been measured in sediment trap material at 100–200 m in the NE Pacific subarctic gyre in summer and fall (0.28–0.44; Wong et al., 2002; Timothy et al., 2013; Dong et al., 2019; see Section 4.3).

4.3. Comparison of ^{234}Th-derived fluxes of major bioelements with other data sets

Fluxes of PN, TPP, bSi, and PIC derived from water column ^{234}Th/^{238}U disequilibrium and in situ pumps are compared to the POC fluxes estimated using the same approach (Buesseler et al., 2020a) and PN, TPP, bSi, and PIC fluxes measured with sediment traps (Estapa et al., 2021) during EXPORTS. These results are also discussed considering previous particle flux studies at Station P and elsewhere.

The clearest feature of EXPORTS biogenic fluxes is the steep and shallow attenuation of the soft tissue-associated POC, PN, and TPP fluxes from 50 m to the base of the euphotic zone (approximately 120 m), in contrast to the little to no significant change in the mineral bSi and PIC fluxes with depth (**Figure 8**). This difference suggests more rapid recycling of organic matter relative to biominerals and is consistent with the general increase in the bSi/POC and PIC/POC flux ratio observed throughout the water column in different regions of the world ocean (Ragueneau et al., 2002; Berelson et al., 2007) and specifically at Station P (Timothy et al., 2013).

Fluxes of PN, TPP, and PIC from 100 to 500 m measured with sediment traps during EXPORTS are similar to those derived from ^{234}Th (Estapa et al., 2021; **Table 4**). In contrast, trap-derived bSi fluxes were generally lower than those measured with ^{234}Th (though we acknowledge the high uncertainties; **Table 4**). These differences are driven by the discrepancy in ^{234}Th fluxes measured by traps and those predicted from ^{234}Th disequilibrium in seawater, as the relative composition of bSi to ^{234}Th in trap particles and the midsized class is very similar. The potential reasons underlying the differences in ^{234}Th-derived particle fluxes are discussed in detail in Estapa et al. (2021), including the undersampling of small (<40 μm) and large particles (>1 mm) by traps and the active transport of ^{234}Th (and other elements) by vertically migrating zooplankton.

Of importance to this study is the summary of 10 years of surface-tethered free-drifting sediment trap data (50–1,000 m, 1987–1998) at Station P by Wong et al. (2002) complemented with additional data to 2005 (Buesseler et al., 2020a), and the climatology of particle flux measured at Station P using moored sediment traps (200, 1,000, and 3,800 m, 1980s–2006) summarized in Timothy et al. (2013). We henceforth refer to the average fluxes obtained from July to September for drifting sediment traps (Wong et al., 2002) and the average seasonal fluxes from summer (mid-May to mid-August) and the fall (mid-August to mid-November) for moored sediment traps (Timothy et al., 2013). Drifting sediment traps show a strong attenuation of PN fluxes from 50 to 100 m and low fluxes at 500 m similar to those measured during EXPORTS (Wong et al., 2002; **Table 4**). Yet, their average PN fluxes above 500 m tend to be higher than in this study, possibly due to swimmer contamination in the trap samples as discussed by Wong et al. (2002). On the other hand, seasonal PN fluxes measured at 200 m with moored sediment traps are 0.09–0.18 mmol N m^{-2} d^{-1} and bSi fluxes are 0.48–1.02 mmol Si m^{-2} d^{-1}, encompassing the ^{234}Th-derived fluxes during EXPORTS (**Table 4**). However, Timothy et al. (2013) reported consistently higher bSi fluxes at 1,000 m than at 200 m, which was hypothesized to be related to a lower trapping efficiency of the shallow trap. Therefore, their bSi and PN fluxes at 200 m should be considered minimum estimates as noted for POC flux.

Regarding PIC, the average fluxes reported by Wong et al. (2002) and Timothy et al. (2013) are strikingly higher than the EXPORTS fluxes by 1 to 2 orders of magnitude (**Table 4**). These higher values are consistent with the PIC fluxes measured with surface-tethered free-drifting sediment traps at 100 and 200 m about 4° west of Station P in August 2017 (0.75–1.03 mmol C m^{-2} d^{-1}; Dong et al., 2019). However, a closer look at the time-series trap data reveals that the PIC fluxes during EXPORTS are similar to the minimum fluxes reported by Wong et al. (2002) and Timothy et al. (2013) in the upper 1,000 m in July–September during their entire period of observations (approximately 0.10 mmol C m^{-2} d^{-1}). PIC fluxes at Station P are mainly composed of coccolithophores, pteropods, and foraminifera (Wong et al., 1999, 2002; Tsurumi et al., 2005; Timothy et al., 2013). We cannot rule out the possibility that trap measurements may in part reflect the presence of live zooplankton, such as small pteropods or shell fragments, that were not part of the passive sinking flux. For example, Wong et al. (1999) reported that 200-m trap samples were frequently impacted by hundreds of swimmers, mostly copepods, amphipods, and pteropods. However, high average PIC/POC ratios found by previous trap studies (Wong et al., 2002; Timothy et al., 2013; Dong et al., 2019) cannot be explained by swimmer contamination because the collection of live pteropods and other zooplankton would bias PIC/POC ratios toward low (rather than high) values. The very low PIC fluxes measured in 2018 compared to the longer time-series trap observations at Station P thus likely reflect underlying differences in community structure. Strong variability in the relative contribution of PIC to total carbon

Table 4. Comparison of fluxes of major bioelements at Station P. DOI: https://doi.org/10.1525/elementa.2020.00166.t4

Bioelement Fluxes	50 m	100 m	150 m	200 m	330 m	500 m
PN fluxes (mmol N m^{-2} d^{-1})						
This study[a]	0.82 ± 0.31	0.28 ± 0.08	0.14 ± 0.06	0.13 ± 0.09	0.15 ± 0.12	0.16 ± 0.17
Estapa et al. (2021)[b]	–			0.23 ± 0.11		
Timothy et al. (2013)[c]	–	–	–	0.09 – 0.18	–	–
Wong et al. (2002)[d]	1.32 ± 0.58	0.59 ± 0.32	–	0.49 ± 0.17	–	0.21 ± 0.06
TPP fluxes (mmol P m^{-2} d^{-1})						
This study[a]	0.191 ± 0.067	0.029 ± 0.008	0.011 ± 0.005	0.009 ± 0.007	0.010 ± 0.008	0.011 ± 0.011
Estapa et al. (2021)[b]	–			0.007 ± 0.007		
bSi fluxes (mmol Si m^{-2} d^{-1})						
This study[a]	0.81 ± 0.23	0.73 ± 0.23	0.61 ± 0.30	0.55 ± 0.40	0.71 ± 0.59	1.06 ± 1.09
Estapa et al. (2021)[b]	–	0.34 ± 0.24	0.26 ± 0.14	0.19 ± 0.09	0.13 ± 0.05	0.16 ± 0.08
Timothy et al. (2013)[c]	–	–	–	0.48 – 1.02	–	–
PIC fluxes (mmol C m^{-2} d^{-1})						
This study[a]	0.047 ± 0.015	0.056 ± 0.020	0.053 ± 0.026	0.047 ± 0.034	0.062 ± 0.051	0.060 ± 0.063
Estapa et al. (2021)[b]	–			0.045 ± 0.025		
Timothy et al. (2013)[c]	–	–	–	0.34 – 0.95	–	–
Wong et al. (2002)[d]	3.76 ± 2.07	2.77 ± 2.32	–	1.14 ± 0.49	–	0.66 ± 0.18

PN = particulate nitrogen; TPP = total particulate phosphorus; bSi = biogenic silica; PIC = particulate inorganic carbon; EXPORTS = EXport Processes in the Ocean from RemoTe Sensing.

[a]^{234}Th-derived cruise-average fluxes during EXPORTS (**Table 3**).

[b]Trap-derived cruise-average (± standard deviation) from three trap deployments (once per epoch) combining surface-tethered traps and neutrally-buoyant sediment traps during EXPORTS. PN, TPP, and PIC fluxes correspond to the average based on seven samples spanning depths from 100 to 500 m.

[c]Range of the average seasonal fluxes from moored traps (1989–2006) in the summer (mid-May to mid-August) and the fall (mid-August to mid-November).

[d]Average (± standard deviation) fluxes from surface-tethered traps (1987–2000) in July–September ($n = 7$ for each depth, except $n = 4$ for 50 m).

production at Station P is illustrated with PIC/POC production ratios ranging from 0.02 to 0.41 in September from 1998 to 2000 (Lipsen et al., 2007). Interannual and intraannual variability in surface PIC concentrations around Station P is clearly shown by satellite observations (NASA Goddard Space Flight Center, 2018). In 2018, PIC concentrations peaked 3 months prior to EXPORTS and concentrations during sampling were a factor of 2 lower than the average time-series concentrations in August and September from 2002 to 2018 (Figure S3). Therefore, August–September 2018 may have been a time of anomalously low PIC production, resulting in low PIC fluxes.

On a broader perspective, Buesseler et al. (2020a) discussed that POC fluxes measured during EXPORTS place Station P as one of the more modest POC flux settings in the global ocean. For example, average POC fluxes derived from ^{234}Th at the base of the euphotic zone during EXPORTS (1.7 ± 0.6 mmol C m^{-2} d^{-1}; Buesseler et al., 2020a) are similar to those measured at 150 m at an oligotrophic station in the central North Pacific (ALOHA) using ^{234}Th and free-drifting and neutrally-buoyant sediment traps (Karl et al., 1996; Benitez-Nelson et al., 2001; Lamborg et al., 2008). The same holds true for PN and TPP fluxes, with the exception of lower TPP fluxes measured with neutrally-buoyant sediment traps at ALOHA during the VERTIGO program (Lamborg et al., 2008). However, PIC fluxes during EXPORTS are toward the low end of those measured at ALOHA (Lamborg et al., 2008). Fluxes of bSi measured at the base of the euphotic zone during EXPORTS are clearly low compared to studies conducted in nonoligotrophic and diatom-dominated areas including the K2 site in the NW Pacific and regions of the Southern Ocean (>10 mmol Si m^{-2} d^{-1}; Buesseler et al., 2001; Buesseler et al., 2008b; Lamborg et al., 2008) but higher than those reported in the Sargasso Sea and at ALOHA during diatom blooms (<0.4 mmol Si m^{-2} d^{-1}; Benitez-Nelson et al., 2007a; Buesseler et al., 2008a; Lamborg et al., 2008).
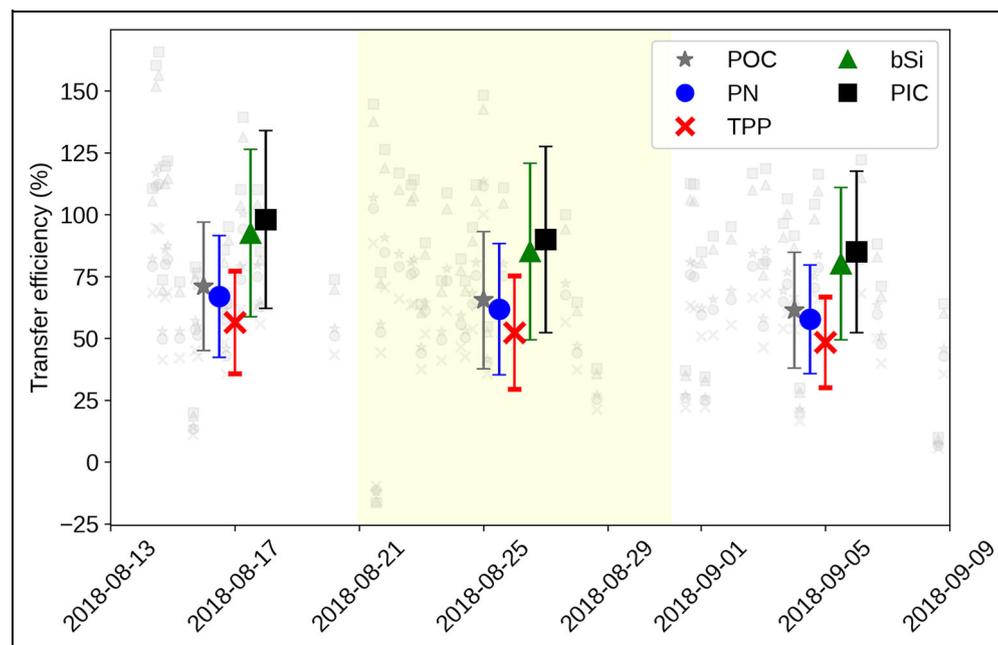
Figure 9. Transfer efficiencies in the upper twilight zone. Mean transfer efficiencies of particulate organic carbon (gray), particulate nitrogen (blue), total particulate phosphorus (red), biogenic silica (green), and particulate inorganic carbon fluxes (black; flux at 220 m/flux at 120 m) using the steady-state fluxes determined at each station sampled for thorium-234 during EXPORTS (Table S3) by sampling "epoch." Error bars show 1 standard deviation of the mean. Left-to-right panels indicate Epochs 1–3 with yellow shading denoting boundaries between epochs; dates are year–month–day. Light gray symbols in the background show data points from individual stations. DOI: https://doi.org/10.1525/elementa.2020.00166.f9

4.4. Biological pump efficiency below the euphotic zone

The transfer efficiency, or T_{100}, is a measure of how efficiently biogenic material is exported through the upper 100 m of the twilight zone in different oceanic regions (Buesseler and Boyd, 2009; Buesseler et al., 2020b). Here, transfer efficiency was calculated by dividing the bioelement fluxes at 220 m by those estimated at the base of the euphotic zone (approximately 120 m, defined by 0.1% PAR and the PPZ; see Methods), as done in Buesseler et al. (2020a) for POC. The bioelement fluxes at 220 m were approximated from the fluxes at 200 m since seawater samples for ^{234}Th analysis were always collected around 200 m and flux gradients within the 200–280 m range were small (**Figure 8**).

The cruise-average transfer efficiencies using the fluxes presented in **Table 3** are 58% $\pm$ 44% for PN, 49% $\pm$ 39% for TPP, 79% $\pm$ 66% for bSi, and 84% $\pm$ 70% for PIC. The cruise-average transfer efficiency for POC was 61% $\pm$ 46% (Buesseler et al., 2020a). Transfer efficiencies measured with traps over the three epochs ranged from 39% to 94% for POC and 41% to 110% for bSi (Estapa et al., 2021), encompassing the cruise-average estimates using ^{234}Th. Transfer efficiencies were also calculated at each station sampled for ^{234}Th during EXPORTS using the steady-state fluxes (Table S3). Considering the data from all stations (**Figure 9**), TPP is the element that shows the lowest transfer efficiency (Mann–Whitney rank-sum test, $P \leq 0.001$ for POC, bSi, and PIC; $P = 0.007$ for PN), followed by PN and POC, which show comparable transfer efficiencies (Mann–Whitney rank-sum test, $P = 0.222$), and finally by bSi and PIC, which are also comparable (Mann–Whitney rank-sum test, $P = 0.247$). Therefore, transfer efficiencies of these major bioelements order as PIC $\sim$ bSi > POC $\sim$ PN > TPP, indicating smaller losses of biominerals compared to organic matter as particles sink. Transfer efficiencies appeared to decrease with time during EXPORTS (**Figure 9**), but this trend is not statistically significant for any element (one-way ANOVA, $P \geq 0.489$).

To our knowledge, this study is the first to report POC, PN, TPP, bSi, and PIC transfer efficiencies in the subarctic NE Pacific. Previous sediment trap studies in this region have focused on a subset of these bioelements and reached different conclusions regarding the attenuation of organic matter versus biominerals within the twilight zone. Wong et al. (2002) found similar transfer efficiencies for POC and PN from 100 to 200 m, but the lowest transfer efficiencies for PIC. Over the same depth range, Dong et al. (2019) found comparable transfer efficiencies for PIC and POC. In deeper waters, Timothy et al. (2013) found higher transfer efficiencies for bSi and PIC compared to POC and PN between 200 and 1,000 m. Therefore, the EXPORTS results and those obtained from moored sediment traps indicate that POC and PN are more rapidly lost than bSi and PIC in the upper water column despite the shallow calcium carbonate saturation horizon in the NE Pacific (Feely et al., 2002).

Studies conducted in other regions of the world ocean support the finding that POC, PN, and TPP are

preferentially remineralized relative to biomineral fluxes in the upper water column (Buesseler et al., 2001; Buesseler et al., 2007a; Lamborg et al., 2008; Engel et al., 2017). This finding is consistent with the view that aggregates containing sufficient amounts of bSi, calcium carbonate, or terrigenous material are more likely to reach the ocean interior than unballasted material by increasing the density and sinking velocity of aggregates and, therefore, limiting their residence time in the water column and the impact of heterotrophic remineralization (De La Rocha and Passow, 2007; Ploug et al., 2008; Iversen and Ploug, 2010).

5. Conclusions

We have presented the distribution of size-fractionated POC, PN, TPP, bSi, PIC, and ^{234}Th concentrations in the upper 500 m of the water column during the EXPORTS field campaign in the subarctic NE Pacific. Concentration profiles are discussed in terms of the major processes controlling particle cycling in the ocean, such as remineralization, (dis)aggregation, and diel vertical migration. We found similar remineralization length scales for POC and PN across all particle size classes from depths of 50–500 m. High bSi/POC ratios in large particles may reflect a significant contribution of highly silicified diatoms to the >51 μm particle pool in the euphotic zone. Low PIC concentrations and PIC/POC ratios suggest a small contribution of coccolithophores to particle stocks in August–September 2018.

Following the same approach as in Buesseler et al. (2020a) for POC flux, we calculated cruise-average ^{234}Th-derived fluxes of PN, TPP, bSi, and PIC associated with sinking particles. The soft tissue-associated POC, PN, and TPP fluxes strongly attenuated within the euphotic zone down to 1.7 ± 0.6 mmol C m^{-2} d^{-1}, 0.22 ± 0.07 mmol N m^{-2} d^{-1}, and 0.019 ± 0.007 mmol P m^{-2} d^{-1} at 120 m. In contrast, bSi and PIC fluxes were similar with depth, with values of 0.69 ± 0.26 mmol Si m^{-2} d^{-1} and 0.055 ± 0.022 mmol C m^{-2} d^{-1} at 120 m. These results are similar to previous work from Station P, with the notable exception of PIC fluxes, which were 1 to 2 orders of magnitude lower than those measured in previous years using sediment traps. Transfer efficiencies within the upper 100 m of the twilight zone were PIC (84%) ~ bSi (79%) > POC (61%) ~ PN (58%) > TPP (49%). These differences indicate preferential remineralization of TPP relative to POC or PN and larger losses of soft tissue relative to biominerals in sinking particles below the euphotic zone. These results provide the foundation for future efforts examining the role of plankton community composition, food-web dynamics, and bSi production, among others, in the transfer of material from the surface ocean to depth in the northeast Pacific Ocean.

Data accessibility statement

Supplemental files

The supplemental files for this article can be found as follows:

Figure S1. Total particulate phosphorus intercomparison. (DOCX)

Figure S2. Particulate inorganic carbon (PIC)/thorium-234 (^{234}Th) ratios in different particle classes. (DOCX)

Figure S3. Time-series satellite particulate inorganic carbon (PIC) concentration around Station P. (DOCX)

Table S1. In situ pump casts near Station P during the EXport Processes in the Ocean from RemoTe Sensing field campaign. (DOCX)

Table S2. Subsample to subsample variability on quartz microfiber filters. (DOCX)

Table S3. Thorium-234 (^{234}Th), particulate organic carbon (POC), particulate nitrogen (PN), total particulate phosphorus (TPP), biogenic silica (bSi), and particulate inorganic carbon (PIC) fluxes for each cast and depth. (XLSX)

Acknowledgments

Competing interests
The authors declare that they have no conflict of interest.

Author contributions
Contributed to conception and design: CBN, LR, KOB.
Contributed to acquisition of data: MRM, CBN, BPU, AMW, SJC, SP, TJH, MLE, KOB.

Contributed to analysis and interpretation of data: MRM, CBN, AMW, SJC, TJH, MLE, KOB.

Drafted and/or revised this article: MRM, CBN, BPU, AMW, SJC, SP, TJH, MLE, LR, KOB.

Approved the submitted version for publication: MRM, CBN, BPU, AMW, SJC, SP, TJH, MLE, LR, KOB.

References

Antia, AN. 2005. Solubilization of particles in sediment traps: Revising the stoichiometry of mixed layer export. *Biogeosciences* **2**(2): 189–204. DOI: http:// dx.doi.org/10.5194/bg-2-189-2005.

Arístegui, J, Gasol, JM, Duarte, CM, Herndl, GJ. 2009. Microbial oceanography of the dark ocean's pelagic realm. *Limnology and Oceanography* **54**(5): 1501– 1529. DOI: http://dx.doi.org/10.4319/lo.2009.54. 5.1501.

Armstrong, RA, Lee, C, Hedges, JI, Honjo, S, Wakeham, SG. 2002. A new, mechanistic model for organic carbon fluxes in the ocean based on the quantitative association of POC with ballast minerals. *Deep Sea Research Part II: Topical Studies in Oceanography* **49**(1–3): 219–236. DOI: http://dx.doi.org/10. 1016/S0967-0645(01)00101-1.

Aspila, KI, Agemian, H, Chau, ASY. 1976. A semi-automated method for the determination of inorganic, organic and total phosphate in sediments. *Analyst* **101**(1200): 187–197. DOI: http://dx.doi. org/10.1039/an9760100187.

Benitez-Nelson, CR, Bidigare, RR, Dickey, TD, Landry, MR, Leonard, CL, Brown, SL, Nencioli, F, Rii, YM, Maiti, K, Becker, JW, Bibby, TS, Black, W, Cai, W-J, **Carlson, CA, Chen, F, Kuwahara, VS, Mahaffey, C, McAndrew, PM, Quay, PD, Rappé, MS, Selph, KE, Simmons, MP, Yang, EJ**. 2007. Mesoscale eddies drive increased silica export in the Subtropical Pacific Ocean. *Science* **316**(5827): 1017–1021. DOI: http://dx.doi.org/10.1126/science.1136221.

Benitez-Nelson, CR, Buesseler, KO, Karl, DM, Andrews, J. 2001. A time-series study of particulate matter export in the North Pacific Subtropical Gyre based on ^{234}Th:^{238}U disequilibrium. *Deep Sea Research Part I: Oceanographic Research Papers* **48**(12): 2595– 2611. DOI: http://dx.doi.org/10.1016/S0967- 0637(01)00032-2.

Benitez-Nelson, CR, O'Neill Madden, LP, Styles, RM, Thunell, RC, Astor, Y. 2007. Inorganic and organic sinking particulate phosphorus fluxes across the oxic/anoxic water column of Cariaco Basin, Venezuela. *Marine Chemistry* **105**(1–2): 90–100. DOI: http:// dx.doi.org/10.1016/J.MARCHEM.2007.01.007.

Berelson, WM, Balch, WM, Najjar, R, Feely, RA, Sabine, C, Lee, K. 2007. Relating estimates of $CaCO_3$ production, export, and dissolution in the water column to measurements of $CaCO_3$ rain into sediment traps and dissolution on the sea floor: A revised global carbonate budget. *Global Biogeochemical Cycles* **21**(GB1024). DOI: http://dx.doi.org/10. 1029/2006GB002803.

Bishop, JKB, Lam, PJ, Wood, TJ. 2012. Getting good particles: Accurate sampling of particles by large volume in-situ filtration. *Limnology and Oceanography Methods* **10**(9): 681–710. DOI: http://dx.doi.org/10. 4319/lom.2012.10.681.

Bishop, JKB, Wood, TJ. 2008. Particulate matter chemistry and dynamics in the twilight zone at VERTIGO ALOHA and K2 sites. *Deep Sea Research Part I: Oceanographic Research Papers* **55**(12): 1684–1706. DOI: http://dx.doi.org/10.1016/J.DSR.2008.07.012.

Bodel, A, Durkin, CA, Buesseler, K, Estapa, ML, Omand, M. 2020. *Sinking cells in the twilight zone and their contribution to carbon export*. San Diego, CA: Ocean Sciences Meeting. Available at https:// agu.confex.com/agu/osm20/meetingapp.cgi/ Paper/655930.

Boyd, PW, Claustre, H, Levy, M, Siegel, DA, Weber, T. 2019. Multi-faceted particle pumps drive carbon sequestration in the ocean. *Nature* **568**(7752): 327–335. DOI: http://dx.doi.org/10.1038/s41586- 019-1098-2.

Brzezinski, MA. 1985. The Si: C: N ratio of marine diatoms: Interspecific variability and the effect of some environmental variables. *Journal of Phycology* **21**(3): 347–357. DOI: http://dx.doi.org/10.1111/j.0022- 3646.1985.00347.x.

Brzezinski, MA, Nelson, DM. 1989. Seasonal changes in the silicon cycle within a Gulf Stream warm-core ring. *Deep Sea Research Part A. Oceanographic Research Papers* **36**(7): 1009–1030. DOI: http://dx. doi.org/10.1016/0198-0149(89)90075-7.

Buesseler, KO, Antia, AN, Chen, M, Fowler, SW, Gardner, WD, Gustafsson, O, Harada, K, Michaels, AF,

Rutgers van der Loeff, M, Sarin, M, Steinberg, DK, Trull, T. 2007b. An assessment of the use of sediment traps for estimating upper ocean particle fluxes. *Journal of Marine Research* **65**(3): 345–416. DOI: http://dx.doi.org/10.1357/00222400778 1567621.

Buesseler, KO, Bacon, MP, Cochran, JK, Livingston, HD. 1992. Carbon and nitrogen export during the JGOFS North Atlantic Bloom experiment estimated from ^{234}Th:^{238}U disequilibria. *Deep Sea Research Part A. Oceanographic Research Papers* **39**(7–8): 1115–1137. DOI: http://dx.doi.org/10.1016/0198-0149 (92)90060-7.

Buesseler, KO, Ball, L, Andrews, J, Benitez-Nelson, C, Belastock, R, Chai, F, Chao, Y. 1998. Upper ocean export of particulate organic carbon in the Arabian Sea derived from thorium-234. *Deep Sea Research Part II: Topical Studies in Oceanography* **45**(10–11): 2461–2487. DOI: http://dx.doi.org/10.1016/S0967-0645(98)80022-2.

Buesseler, KO, Ball, L, Andrews, J, Cochran, JK, Hirschberg, DJ, Bacon, MP, Fleer, A, Brzezinski, M. 2001. Upper ocean export of particulate organic carbon and biogenic silica in the Southern Ocean along 170°W. *Deep Sea Research Part II: Topical Studies in Oceanography* **48**(19–20): 4275–4297. DOI: http://dx.doi.org/10.1016/S0967-0645(01)00089-3.

Buesseler, KO, Benitez-Nelson, CR, Moran, SB, Burd, A, Charette, M, Cochran, JK, Coppola, L, Fisher, NS, Fowler, SW, Gardner, WD, Guo, LD, Gustafsson, Ö, Lamborg, C, Masque, P, Miquel, JC, Passow, U, Santschi, PH, Savoye, N, Stewart, G, Trull, T. 2006. An assessment of particulate organic carbon to thorium-234 ratios in the ocean and their impact on the application of ^{234}Th as a POC flux proxy. *Marine Chemistry* **100**(3–4): 213–233. DOI: http://dx.doi.org/10.1016/j.marchem.2005.10.013.

Buesseler, KO, Benitez-Nelson, CR, Roca-Martí, M, Wyatt, AM, Resplandy, L, Clevenger, SJ, Drysdale, JA, Estapa, ML, Pike, S, Umhau, BP. 2020a. High-resolution spatial and temporal measurements of particulate organic carbon flux using thorium-234 in the northeast Pacific Ocean during the EXport Processes in the Ocean from RemoTe Sensing field campaign. *Elementa: Science of the Anthropocene* **8**(1): 030. DOI: http://dx.doi.org/10.1525/elementa.030.

Buesseler, KO, Boyd, PW. 2009. Shedding light on processes that control particle export and flux attenuation in the twilight zone of the open ocean. *Limnology and Oceanography* **54**(4): 1210–1232. DOI: http://dx.doi.org/10.4319/lo.2009.54.4.1210.

Buesseler, KO, Boyd, PW, Black, EE, Siegel, DA. 2020b. Metrics that matter for assessing the ocean biological carbon pump. *Proceedings of the National Academy of Sciences* **117**(18): 9679–9687. DOI: http://dx.doi.org/10.1073/PNAS.1918114117.

Buesseler, KO, Lamborg, CH, Boyd, PW, Lam, PJ, Trull, TW, Bidigare, RR, Bishop, JKB, Casciotti, KL, Dehairs, F, Elskens, M, Honda, M, Karl, DM, Siegel, DA, Silver, MW, Steinberg, DK, Valdes, J, Van Mooy, B, Wilson, S. 2007a. Revisiting carbon flux through the ocean's twilight zone. *Science* **316**(5824): 567–570. DOI: http://dx.doi.org/10.1126/science.1137959.

Buesseler, KO, Lamborg, CH, Cai, P, Escoube, R, Johnson, R, Pike, S, Masque, P, McGillicuddy, D, Verdeny, E. 2008a. Particle fluxes associated with mesoscale eddies in the Sargasso Sea. *Deep Sea Research Part II: Topical Studies in Oceanography* **55**(10–13): 1426–1444. DOI: http://dx.doi.org/10.1016/j.dsr2.2008.02.007.

Buesseler, KO, Trull, TW, Steinberg, DK, Silver, MW, Siegel, DA, Saitoh, S-I, Lamborg, CH, Lam, PJ, Karl, DM, Jiao, NZ, Honda, MC, Elskens, M, Dehairs, F, Brown, SL, Boyd, PW, Bishop, JKB, Bidigare, RR. 2008b. VERTIGO (VERtical Transport in the Global Ocean): A study of particle sources and flux attenuation in the North Pacific. *Deep Sea Research Part II: Topical Studies in Oceanography* **55**(14–15): 1522–1539. DOI: http://dx.doi.org/10.1016/j.dsr2.2008.04.024.

Cutter, G, Casciotti, K, Croot, P, Geibert, W, Heimbürger, L-E, Lohan, M, Planquette, H, van de Flierdt, T. 2017. Sampling and Sample-handling Protocols for GEOTRACES Cruises. Version 3.0. Toulouse, France, GEOTRACES International Project Office. DOI: http://dx.doi.org/10.25607/OBP-2.

De La Rocha, CL, Passow, U. 2007. Factors influencing the sinking of POC and the efficiency of the biological carbon pump. *Deep Sea Research Part II: Topical Studies in Oceanography* **54**(5–7): 639–658. DOI: http://dx.doi.org/10.1016/j.dsr2.2007.01.004.

Dong, S, Berelson, WM, Rollins, NE, Subhas, AV, Naviaux, JD, Celestian, AJ, Liu, X, Turaga, N, Kemnitz, NJ, Byrne, RH, Adkins, JF. 2019. Aragonite dissolution kinetics and calcite/aragonite ratios in sinking and suspended particles in the North Pacific. *Earth and Planetary Science Letters* **515**: 1–12. DOI: http://dx.doi.org/10.1016/j.epsl.2019.03.016.

Ehrhardt, M, Koeve, W. 1999. Determination of particulate organic carbon and nitrogen, in Grasshoff K, Kremling K, Ehrhardt M eds., *Methods of seawater analysis*. Third edition. Weinheim, Germany: Wiley: 437–444.

Engel, A, Wagner, H, Le Moigne, FAC, Wilson, ST. 2017. Particle export fluxes to the oxygen minimum zone of the eastern tropical North Atlantic. *Biogeosciences* **14**(7): 1825–1838. DOI: http://dx.doi.org/10.5194/bg-14-1825-2017.

Estapa, M, Buesseler, K, Durkin, CA, Omand, M, Benitez-Nelson, CR, Roca-Martí, M, Breves, E, Kelly, RP, Pike, S. 2021. Biogenic sinking particle fluxes and sediment trap collection efficiency at Ocean Station Papa. *Elementa: Science of the Anthropocene* **9**(1). DOI: https://doi.org/10.1525/elementa.2020.00122.

Feely, RA, Sabine, CL, Lee, K, Millero, FJ, Lamb, MF, Greeley, D, Bullister, JL, Key, RM, Peng, T-H, Kozyr, A, Ono, T, Wong, CS. 2002. In situ calcium

carbonate dissolution in the Pacific Ocean. *Global Biogeochemical Cycles* **16**(4): 1144. DOI: http://dx.doi.org/10.1029/2002gb001866.

Firme, GF, Rue, EL, Weeks, DA, Bruland, KW, Hutchins, DA. 2003. Spatial and temporal variability in phytoplankton iron limitation along the California coast and consequences for Si, N, and C biogeochemistry. *Global Biogeochemical Cycles* **17**(1). DOI: http://dx.doi.org/10.1029/2001GB001824.

Gustafsson, Ö, Gschwend, PM, Buesseler, KO. 1997. Using [234]Th disequilibria to estimate the vertical removal rates of polycyclic aromatic hydrocarbons from the surface ocean. *Marine Chemistry* **57**(1–2): 11–23. DOI: http://dx.doi.org/10.1016/S0304-4203(97)00011-X.

Harrison, PJ. 2002. Station Papa time series: Insights into ecosystem dynamics. *Journal of Oceanography* **58**(2): 259–264. DOI: http://dx.doi.org/10.1023/A:1015857624562.

Honjo, S, Dymond, J, Collier, R, Manganini, SJ. 1995. Export production of particles to the interior of the equatorial Pacific Ocean during the 1992 EqPac experiment. *Deep Sea Research Part II: Topical Studies in Oceanography* **42**(2–3): 831–870. DOI: http://dx.doi.org/10.1016/0967-0645(95)00034-N.

Honjo, S, Manganini, SJ, Krishfield, RA, Francois, R. 2008. Particulate organic carbon fluxes to the ocean interior and factors controlling the biological pump: A synthesis of global sediment trap programs since 1983. *Progress in Oceanography* **76**(3): 217–285. DOI: http://dx.doi.org/10.1016/j.pocean.2007.11.003.

Hutchins, DA, Bruland, KW. 1998. Iron-limited diatom growth and Si: N uptake ratios in a coastal upwelling regime. *Nature* **393**(6685): 561–564. DOI: http://dx.doi.org/10.1038/31203.

Iversen, MH, Ploug, H. 2010. Ballast minerals and the sinking carbon flux in the ocean: Carbon-specific respiration rates and sinking velocity of marine snow aggregates. *Biogeosciences* **7**(9): 2613–2624. DOI: http://dx.doi.org/10.5194/bg-7-2613-2010.

Karl, DM, Christian, JR, Dore, JE, Hebel, DV, Letelier, RM, Tupas, LM, Winn, CD. 1996. Seasonal and interannual variability in primary production and particle flux at station ALOHA. *Deep Sea Research Part II: Topical Studies in Oceanography* **43**(2–3): 539–568. DOI: http://dx.doi.org/10.1016/0967-0645(96)00002-1.

Kiørboe, T. 2000. Colonization of marine snow aggregates by invertebrate zooplankton: Abundance, scaling, and possible role. *Limnology and Oceanography* **45**(2): 479–484. DOI: http://dx.doi.org/10.4319/lo.2000.45.2.0479.

Klaas, C, Archer, DE. 2002. Association of sinking organic matter with various types of mineral ballast in the deep sea: Implications for the rain ratio. *Global Biogeochemical Cycles* **16**(4): 1116. DOI: http://dx.doi.org/10.1029/2001GB001765.

Kwon, EY, Primeau, F, Sarmiento, JL. 2009. The impact of remineralization depth on the air–sea carbon balance. *Nature Geoscience* **2**(9): 630–635. DOI: http://dx.doi.org/10.1038/ngeo612.

Lam, PJ, Lee, J-M, Heller, MI, Mehic, S, Xiang, Y, Bates, NR. 2018. Size-fractionated distributions of suspended particle concentration and major phase composition from the U.S. GEOTRACES Eastern Pacific Zonal Transect (GP16). *Marine Chemistry* **201**: 90–107. DOI: http://dx.doi.org/10.1016/j.marchem.2017.08.013.

Lam, PJ, Marchal, O. 2015. Insights into particle cycling from thorium and particle data. *Annual Review of Marine Science* **7**: 159–184. Annual Reviews. DOI: http://dx.doi.org/10.1146/annurev-marine-010814-015623.

Lam, PJ, Ohnemus, DC, Auro, ME. 2015. Size-fractionated major particle composition and concentrations from the US GEOTRACES North Atlantic Zonal Transect. *Deep Sea Research Part II: Topical Studies in Oceanography* **116**: 303–320. DOI: http://dx.doi.org/10.1016/J.DSR2.2014.11.020.

Lamborg, CH, Buesseler, KO, Valdes, J, Bertrand, CH, Bidigare, R, Manganini, S, Pike, S, Steinberg, D, Trull, T, Wilson, S. 2008. The flux of bio- and lithogenic material associated with sinking particles in the mesopelagic "twilight zone" of the northwest and North Central Pacific Ocean. *Deep Sea Research Part II: Topical Studies in Oceanography* **55**(14–15): 1540–1563. DOI: http://dx.doi.org/10.1016/J.DSR2.2008.04.011.

Le Moigne, FAC, Henson, SA, Sanders, RJ, Madsen, E. 2013. Global database of surface ocean particulate organic carbon export fluxes diagnosed from the [234]Th technique. *Earth System Science Data* **5**(2): 295–304. DOI: http://dx.doi.org/10.5194/essd-5-295-2013.

Le Moigne, FAC, Sanders, RJ, Villa-Alfageme, M, Martin, AP, Pabortsava, K, Planquette, H, Morris, PJ, Thomalla, SJ. 2012. On the proportion of ballast versus non-ballast associated carbon export in the surface ocean. *Geophysical Research Letters* **39**(15): L15610. DOI: http://dx.doi.org/10.1029/2012GL052980.

Lipsen, MS, Crawford, DW, Gower, J, Harrison, PJ. 2007. Spatial and temporal variability in coccolithophore abundance and production of PIC and POC in the NE subarctic Pacific during El Niño (1998), La Niña (1999) and 2000. *Progress in Oceanography* **75**(2): 304–325. DOI: http://dx.doi.org/10.1016/j.pocean.2007.08.004.

Lomas, MW, Baer, SE, Acton, S, Krause, JW. 2019. Pumped Up by the Cold: Elemental Quotas and Stoichiometry of Cold-Water Diatoms. *Frontiers in Marine Science* **6**: 286. DOI: http://dx.doi.org/10.3389/fmars.2019.00286.

Maiti, K, Buesseler, KO, Pike, SM, Benitez-Nelson, C, Cai, P, Chen, W, Cochran, K, Dai, M, Dehairs, F, Gasser, B, Kelly, RP, Masque, P, Miller, LA, Miquel, JC, Moran, SB, Morris, PJ, Peine, F, Planchon, F, Renfro, AA, Rutgers van der Loeff, M, Santschi, PH, Turnewitsch, R, Waples, JT, Xu, C.

2012. Intercalibration studies of short-lived thorium-234 in the water column and marine particles. *Limnology and Oceanography Methods* **10**(9): 631–644. DOI: http://dx.doi.org/10.4319/lom.2012.10.631.

Marchetti, A, Cassar, N. 2009. Diatom elemental and morphological changes in response to iron limitation: A brief review with potential paleoceanographic applications. *Geobiology* **7**(4): 419–431. DOI: http://dx.doi.org/10.1111/j.1472-4669.2009.00207.x.

Martiny, AC, Pham, CTA, Primeau, FW, Vrugt, JA, Moore, JK, Levin, SA, Lomas, MW. 2013. Strong latitudinal patterns in the elemental ratios of marine plankton and organic matter. *Nature Geoscience* **6**(4): 279–283. DOI: http://dx.doi.org/10.1038/ngeo1757.

Martiny, AC, Vrugt, JA, Lomas, MW. 2014. Concentrations and ratios of particulate organic carbon, nitrogen, and phosphorus in the global ocean. *Scientific Data* **1**: 140048. DOI: http://dx.doi.org/10.1038/sdata.2014.48.

NASA Goddard Space Flight Center, Ocean Biology Processing Group. 2018. *Moderate-resolution imaging spectroradiometer (MODIS) aqua particulate inorganic carbon data.* NASA OB.DAAC, Greenbelt, MD, USA. DOI: http://doi.org/10.5067/AQUA/MODIS/L3M/PIC/2018. Accessed 1 October 2020. Maintained by NASA Ocean Biology Distributed Active Archive Center (OB.DAAC), Goddard Space Flight Center, Greenbelt MD.

Owens, SA, Pike, S, Buesseler, KO. 2015. Thorium-234 as a tracer of particle dynamics and upper ocean export in the Atlantic Ocean. *Deep Sea Research Part II: Topical Studies in Oceanography* **116**: 42–59. DOI: http://dx.doi.org/10.1016/j.dsr2.2014.11.010.

Ploug, H, Grossart, H-P, Azam, F, Jørgensen, BB. 1999. Photosynthesis, respiration, and carbon turnover in sinking marine snow from surface waters of Southern California Bight: Implications for the carbon cycle in the ocean. *Marine Ecology Progress Series* **179**(11): 1–11. DOI: http://dx.doi.org/10.3354/meps179001.

Ploug, H, Iversen, MH, Fischer, G. 2008. Ballast, sinking velocity, and apparent diffusivity within marine snow and zooplankton fecal pellets: Implications for substrate turnover by attached bacteria. *Limnology and Oceanography* **53**(5): 1878–1886. DOI: http://dx.doi.org/10.4319/lo.2008.53.5.1878.

Price, NM. 2005. The elemental stoichiometry and composition of an iron-limited diatom. *Limnology and Oceanography* **50**(4): 1159–1171. DOI: http://dx.doi.org/10.4319/lo.2005.50.4.1159.

Puigcorbé, V, Masqué, P, Le Moigne, FAC. 2020. Global database of ratios of particulate organic carbon to thorium-234 in the ocean: Improving estimates of the biological carbon pump. *Earth System Science Data* **12**(2): 1267–1285. DOI: http://dx.doi.org/10.5194/essd-12-1267-2020.

Ragueneau, O, Dittert, N, Pondaven, P, Tréguer, P, Corrin, L. 2002. Si/C decoupling in the world ocean: Is the Southern Ocean different? *Deep Sea Research Part II: Topical Studies in Oceanography* **49**(16): 3127–3154. DOI: http://dx.doi.org/10.1016/S0967-0645(02)00075-9.

Siegel, DA, Buesseler, KO, Behrenfeld, MJ, Benitez-Nelson, CR, Boss, E, Brzezinski, MA, Burd, A, Carlson, CA, D'Asaro, EA, Doney, SC, Perry, MJ, Stanley, RHR, Steinberg, DK. 2016. Prediction of the export and fate of global ocean net primary production: The EXPORTS science plan. *Frontiers in Marine Science* **3**: 22. DOI: http://dx.doi.org/10.3389/fmars.2016.00022.

Siegel, DA, Cetinić, I, Graff, JR, Lee, CM, Nelson, N, Perry, MJ, Soto Ramos, I, Steinberg, DK, Buesseler, K, Hamme, R, Fassbender, AJ, Nicholson, D, Omand, MM, Robert, M, Thompson, A, Amaral, V, Behrenfeld, M, Benitez-Nelson, C, Bisson, K, Boss, E, Boyd, PW, Brzezinski, M, Buck, K, Burd, A, Burns, S, Caprara, S, Carlson, C, Cassar, N, Close, H, D'Asaro, E, Durkin, C, Erickson, Z, Estapa, ML, Fields, E, Fox, J, Freeman, S, Gifford, S, Gong, W, Gray, D, Guidi, L, Haëntjens, N, Halsey, K, Huot, Y, Hansell, D, Jenkins, B, Karp-Boss, L, Kramer, S, Lam, P, Lee, J-M, Maas, A, Marchal, O, Marchetti, A, McDonnell, A, McNair, H, Menden-Deuer, S, Morison, F, Niebergall, AK, Passow, U, Popp, B, Potvin, G, Resplandy, L, Roca-Martí, M, Roesler, C, Rynearson, T, Traylor, S, Santoro, A, Seraphin, KD, Sosik, HM, Stamieszkin, K, Stephens, B, Tang, W, Van Mooy, B, Xiong, Y, Zhang, X. 2021. An operational overview of the EXport Processes in the Ocean from RemoTe Sensing (EXPORTS) Northeast Pacific Field Deployment. *Elementa Science of the Anthropocene* **9**(1). DOI: https://doi.org/10.1525/elementa.2020.00107

Steinberg, DK, Landry, MR. 2017. Zooplankton and the ocean carbon cycle. *Annual Review of Marine Science* **9**: 413–444. DOI: http://dx.doi.org/10.1146/annurev-marine-010814-015924.

Strickland, JDH, Parsons, TR. 1972. *A practical handbook of seawater analysis. Bulletin 167 (Second Edition).* Stevenson, JC, Watson, J, Reinhart, JM, Cook, DG, eds., Ottawa, Canada: Fisheries Research Board of Canada, 310 pp.

Teng, Y-C, Primeau, FW, Moore, JK, Lomas, MW, Martiny, AC. 2014. Global-scale variations of the ratios of carbon to phosphorus in exported marine organic matter. *Nature Geoscience* **7**(12): 895–898. DOI: http://dx.doi.org/10.1038/ngeo2303.

Timothy, DA, Wong, CS, Barwell-Clarke, JE, Page, JS, White, LA, Macdonald, RW. 2013. Climatology of sediment flux and composition in the subarctic Northeast Pacific Ocean with biogeochemical implications. *Progress in Oceanography* **116**: 95–129. DOI: http://dx.doi.org/10.1016/J.POCEAN.2013.06.017.

Tsurumi, M, Mackas, DL, Whitney, FA, DiBacco, C, Galbraith, MD, Wong, CS. 2005. Pteropods, eddies,

carbon flux, and climate variability in the Alaska Gyre. *Deep Sea Research Part II: Topical Studies in Oceanography* **52**(7–8): 1037–1053. DOI: http://dx.doi.org/10.1016/j.dsr2.2005.02.005.

Twining, BS, Baines, SB, Fisher, NS. 2004. Element stoichiometries of individual plankton cells collected during the Southern Ocean Iron Experiment (SOFeX). *Limnology and Oceanography* **49**(6): 2115–2128. DOI: http://dx.doi.org/10.4319/lo.2004.49.6.2115.

Twining, BS, Nodder, SD, King, AL, Hutchins, DA, LeCleir, GR, DeBruyn, JM, Maas, EW, Vogt, S, Wilhelm, SW, Boyd, PW. 2014. Differential remineralization of major and trace elements in sinking diatoms. *Limnology and Oceanography* **59**(3): 689–704. DOI: http://dx.doi.org/10.4319/lo.2014.59.3.0689.

Weinstein, SE, Moran, SB. 2005. Vertical flux of particulate Al, Fe, Pb, and Ba from the upper ocean estimated from ^{234}Th/^{238}U disequilibria. *Deep Sea Research Part I: Oceanographic Research Papers* **52**(8): 1477–1488. DOI: http://dx.doi.org/10.1016/j.dsr.2005.03.008.

Wong, CS, Waser, NAD, Whitney, FA, Johnson, WK, Page, JS. 2002. Time-series study of the biogeochemistry of the North East subarctic Pacific: Reconciliation of the C_{org}/N remineralization and uptake ratios with the Redfield ratios. *Deep Sea Research Part II: Topical Studies in Oceanography* **49**(24–25): 5717–5738. DOI: http://dx.doi.org/10.1016/S0967-0645(02)00211-4.

Wong, CS, Whitney, FA, Crawford, DW, Iseki, K, Matear, RJ, Johnson, WK, Page, JS, Timothy, D. 1999. Seasonal and interannual variability in particle fluxes of carbon, nitrogen and silicon from time series of sediment traps at Ocean Station P, 1982–1993: Relationship to changes in subarctic primary productivity. *Deep Sea Research Part II: Topical Studies in Oceanography* **46**(11–12): 2735–2760. DOI: http://dx.doi.org/10.1016/S0967-0645(99)00082-X.

Zhang, S-F, Yuan, C-J, Chen, Y, Lin, L, Wang, D-Z. 2019. Transcriptomic response to changing ambient phosphorus in the marine dinoflagellate *Prorocentrum donghaiense*. *Science of the Total Environment* **692**: 1037–1047. DOI: http://dx.doi.org/10.1016/j.scitotenv.2019.07.291.

ELEMENTA
Science of the Anthropocene

Elem Sci Anth is a peer-reviewed open access journal published by University of California Press.

OPEN ACCESS